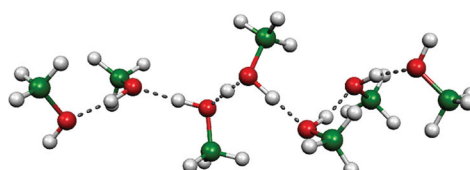
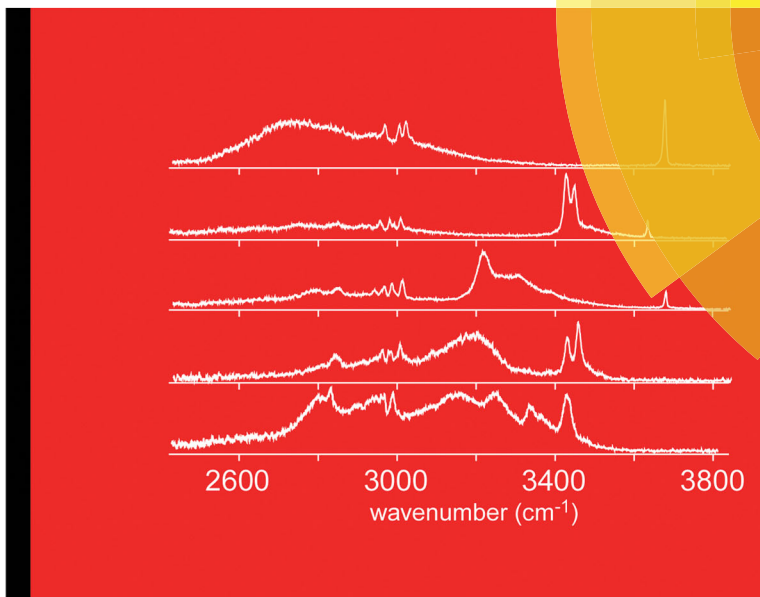
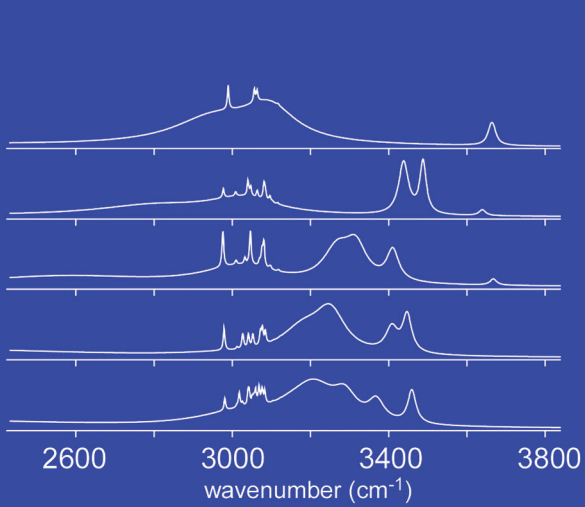


PCCP

Physical Chemistry Chemical Physics
rsc.li/pccp



ISSN 1463-9076



PERSPECTIVE

Asuka Fujii, Jer-Lai Kuo *et al.*
Hydrogen bond network structures of protonated short-chain alcohol clusters



Cite this: *Phys. Chem. Chem. Phys.*,
2018, **20**, 14971

Hydrogen bond network structures of protonated short-chain alcohol clusters†

Asuka Fujii, *^a Natsuko Sugawara,^a Po-Jen Hsu, ^b Takuto Shimamori,^a Ying-Cheng Li, ^b Toru Hamashima^a and Jer-Lai Kuo *^b

Because of the hydrogen bond coordination properties of alcohols, their possible hydrogen bond network structures are categorized into only a few types. Therefore, gas phase clusters of alcohols can be a very simple model system to examine the properties of hydrogen bond networks, such as structural development with cluster size and temperature dependence. In this perspective, we focus on the structural study of protonated short-chain alcohol clusters, whose excess protons (charge) enable size-selective spectroscopy in combination with mass spectrometric techniques. Size-selective infrared spectroscopy and a theoretical multi-scale isomer search were applied to protonated clusters of methanol, which is a prototype of short-chain alcohols, and their hydrogen bond network development is elucidated in detail. Complete isomer population switching with increasing temperature was predicted by the quantum harmonic superposition approximation and this isomer switching was evidenced by the remarkable temperature (internal vibrational energy) dependence of the observed infrared spectra. The characteristics of the temperature dependence of protonated methanol were compared with those of water and neutral methanol. In addition, possible hydrogen bond networks of methanolated ions were discussed on the basis of the results for protonated methanol. Stepwise changes in the internal energy of clusters with inert gas tagging are demonstrated. Convergence of the hydrogen bond network to the bulk-like network in large clusters is also discussed. The hydrogen bond structures of the protonated clusters of longer normal alkyl chain alcohols (ethanol, 1-propanol, 1-butanol, and 1-pentanol) are determined by comparison of their infrared spectra with those of the protonated methanol clusters. It is demonstrated that the normal alkyl chain interferes only slightly with the most stable hydrogen bond structure, although a few exceptional cases were also found. These exception cases serve as good model systems for further theoretical and computational studies.

Received 1st December 2017,
Accepted 5th March 2018

DOI: 10.1039/c7cp08072g

rsc.li/pccp

I. Introduction

Short-chain alcohols are important solvents in chemistry and biochemistry.¹ Their properties as protic and polar solvents are attributed to their hydroxyl groups and their hydrogen bond (H-bond) abilities. For a single hydroxyl group with two lone pairs in an alcohol molecule, the maximum H-bond coordination number is restricted to three (single donor–double acceptor). In H-bond networks between alcohol molecules,^{2–26} two-coordination (single donor–single acceptor) is preferred because of the stoichiometry of the proton donor and acceptor sites. Thus, the H-bond network structures of alcohols are much simpler than those

of water, which can be four-coordinated (double donor–double acceptor). Therefore, alcohol clusters in the gas phase can be a very simple model system to explore the microscopic picture of H-bond networks, which will be crucial to understand complicated bulk systems.^{27–47} While H-bond network structures (potential landscape) of water clusters are so complicated that a systematic understanding of these structures is still very difficult,^{48–51} the H-bond networks of alcohol clusters can be categorized into only a few structure types.^{52–57} The restricted variety of H-bonded networks in alcohols suppresses the number of stable structural isomers of alcohol clusters. Therefore, as demonstrated in this perspective, H-bonded networks of alcohol clusters show remarkable dependence on important physical factors, such as size and temperature. Thus, alcohol clusters are a highly useful prototype to extract the physical essence of the nature of H-bonded networks.

Protonated alcohol clusters are of special importance.^{52–70} Size selection has been the most serious technical problem in cluster studies. The excess charge of protonated clusters enables

^a Department of Chemistry, Graduate School of Science, Tohoku University, Sendai 980-8578, Japan. E-mail: asukafujii@m.tohoku.ac.jp

^b Institute of Atomic and Molecular Sciences, Academia Sinica, Taipei 10617, Taiwan. E-mail: jlkuo@pub.iams.sinica.edu.tw

† Electronic supplementary information (ESI) available. See DOI: 10.1039/c7cp08072g

definite selection of the size of the cluster by mass spectrometric techniques. Temperature control of neutral clusters is also a very difficult task at present.^{71–75} However, various experimental techniques for temperature control, such as inert gas tagging and cryogenic ion trapping, can be applied to protonated (charged) clusters.^{54,56,57,76–96} In addition, protonated clusters provide detailed information on excess proton solvation in protic solvents, such as the competition between the Eigen and Zundel forms in the Grotthuss mechanism.^{50,51,60–63,65,66,79,97–106} The protonated site of alcohols has a special H-bonded coordination character (double donor). This induces some H-bonded network structures that are characteristic of protonated alcohol clusters.^{52–56,69,70} Comparison between the H-bond networks of protonated methanol and methanolated ions, which have been extensively studied, is also of great interest.^{107–120}

The most fundamental factor in a molecular cluster is its size. With increasing cluster size, more complicated intermolecular structures can be formed. The development of size-dependent H-bonded networks of protonated alcohol clusters has been extensively studied, especially in protonated methanol clusters, $H^+(MeOH)_n$, which are the simplest prototype of protonated alcohols.^{52–61,64–70} The H-bonded network structures of $H^+(MeOH)_n$ have been explored both by experimental and theoretical approaches. They are categorized into four types according to the topological consideration of the H-bond coordination properties.^{52–56,69,70} Up to $n = 7$, all the possible H-bond network types have been experimentally observed, and further size development simply results in expansion of the basic network motifs. Therefore, clusters of relatively small regions ($n \leq 7$) can fully provide a basis for discussion of the H-bond network properties of protonated alcohols.

The preferred H-bonded network structure of a cluster depends not only on its size but also on temperature.^{71–96,121–132} Most chemical and biochemical issues concerning H-bonds assume room temperature conditions. To fully understand the properties of the H-bond network of the cluster, therefore, determination of the minimum energy structure is insufficient, and the temperature dependence of the preferred structure is essential. After we survey the possible isomer structures of the cluster, the temperature dependence of the preferred structure can be theoretically predicted by statistical mechanics. In the case of neutral clusters, however, control of their temperature is still practically very difficult. Although many theoretical predictions have been made, their experimental confirmation has been very rare.^{71–75} On the other hand, temperature change of protonated (ionic) clusters is relatively easily achieved by inert gas tagging, and the recent development of the cryogenic ion trap technique enables full control of the temperature.^{76–96} The H-bonded networks of protonated alcohols show remarkable temperature dependence because their variety is restricted. In $H^+(MeOH)_n$, complete switching of the isomer population with increasing temperature has been observed.^{54,56,57,70} This isomer population switching of the clusters corresponds to the phase change in the bulk, and it clearly demonstrates the importance of temperature in H-bonded networks.

Structure studies of (protonated) methanol clusters have only focused on their H-bonded structures. However, short-chain

alcohols are actually amphiphilic. Their alkyl chains introduce non-polarity to the alcohols. The major interaction with the alkyl group is due to dispersion; it plays an essential role in the dissolution of hydrophobic compounds and in crystalline packing. Because the magnitude of dispersion increases with increasing alkyl chain length, dispersion among the alkyl chains becomes more competitive with the H-bond localized at the hydroxyl group in longer-chain alcohols. In the case of bulky alkyl (or aromatic) groups, steric repulsion can also be an important factor to determine the intermolecular structures of alcohols. An example is seen in crystalline structures; while the crystal of methanol is composed of nearly linear H-bonded chains, helical chains or short rings are seen in crystals of some alcohols with bulky groups.^{133–136} Very different H-bond network motifs for liquid methanol and bulk alcohol have been predicted by the quantum cluster equilibrium model approach.^{20,137,138} Most of the structural studies on alcohol clusters have focused only on methanol clusters. However, studies of the competition between H-bonds and van der Waals interactions are rare for gas phase clusters. Recently, structures of cyclohexanol clusters have been studied to examine this competition.^{139,140}

The combination of experimental and theoretical methods, *i.e.*, size-selective infrared (IR) spectroscopy and quantum chemical computations, is a powerful approach to explore the structures of alcohol clusters because their OH stretching vibrations sensitively reflect their H-bonded structures. In this perspective, we review our IR and theoretical studies of protonated methanol clusters^{52–57} and present a new extension to longer-chain alcohols. First, we discuss the topological categorization of possible H-bonded networks of protonated alcohols. Second, the H-bonded structures of $H^+(MeOH)_n$ are discussed as a prototype of alcohols.^{52,53,56} For the size region of $n = 4$ to 8, in which multiple structure types can compete with each other, the multi-scale approach is applied to extensively search for stable isomer structures.^{47,141–143} IR spectra are measured under two different internal energy conditions and are interpreted according to the temperature dependence of the isomer type populations.^{54,56} The results are compared with those of water and neutral methanol. Implications for the H-bond networks of methanolated ions are also discussed. Third, the stepwise internal energy change of $H^+(MeOH)_{5,7}$ is demonstrated using inert gas tagging.⁵⁷ Fourth, the H-bonded networks of large protonated methanol clusters are characterized by the convergence of their IR spectra with cluster size.⁵⁵ A comparison with the spectra of bulk methanol is also shown. Finally, we present newly measured IR spectra and calculated data of longer normal-chain protonated alcohols (ethanol, 1-propanol, 1-butanol, and 1-pentanol). We discuss how the interactions between the normal alkyl chains compete with H-bonds between the hydroxyl groups.

II. H-Bond network structure types in protonated alcohol clusters

Prior to the presentation of the experimental and calculation results, we will first review the topological development of

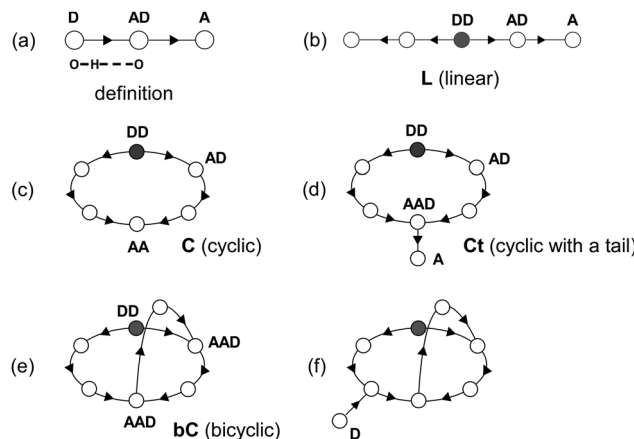


Fig. 1 Schematics of the hydrogen bonds (H-bonds) and H-bond network structures of protonated methanol (alcohol) clusters. (a) Definitions of the symbols. An open circle represents a methanol molecule, and a line between circles indicates an H-bond. An arrow represents the direction of the H-bond (from the proton donor to the acceptor). (b–e) Examples of linear (**L**), cyclic (**C**), cyclic with a tail (**Ct**), and bicyclic (**bC**) type structures, respectively. (f) Side chain formation following the completion of a **bC** type structure. Single proton donor, single acceptor, double acceptor, and double acceptor–single donor sites are denoted as D, A, AD, AA, and AAD, respectively. The protonated site is a double proton donor (DD) site and is represented by a filled circle.

possible H-bond networks in neutral and protonated alcohol clusters.^{52,53,56} In the following, we tentatively assume the case of methanol; however, the same discussion can be applied to other alcohols, as shown later in Section VIII. The schematics of the H-bond networks are shown in Fig. 1. The definition of the scheme is shown in Fig. 1(a). A circle represents a methanol (alcohol) molecule. A line between circles corresponds to an H-bond, and its arrow represents the direction of the H-bond (from the proton donor to the acceptor). Because we focus on the structures of H-bonded networks, all the methyl (alkyl) groups and their conformations are ignored in this scheme. Molecules in a hydrogen bond network can be categorized into several types according to H-bond coordination number. In Fig. 1(a), three different types of molecules are shown; each terminal molecule plays the role only of a proton donor (D) or of an acceptor (A). The A site molecule retains a free OH group and can donate its proton to form a new hydrogen bond. The central molecule is not only a proton donor but also an acceptor; this molecule is called an acceptor–donor (AD).

The simplest H-bond network type in protonated methanol is a linear H-bond chain (**L**), as seen in Fig. 1(b). In the protonated clusters, the protonated site (ion core) has unique coordination properties. Both the Eigen type (CH_3OH_2^+) and Zundel type ($\text{CH}_3\text{OH}-\text{H}^+-(\text{CH}_3\text{OH})$) ion cores can be double donor (DD) sites. From the central DD site, two linear chains extend. Both terminals of the **L** type structure of $\text{H}^+(\text{MeOH})_n$ are A sites. AD sites can exist between the DD and A sites, and the number of AD sites is determined by the cluster size. When the two terminals of an **L** type structure are bound to each other, a cyclic (**C**) type structure is formed (Fig. 1(c)). Here, we should note that the binding site becomes a double acceptor (AA) site, and it has a free OH. The **C**

type can be formed at $n \geq 4$; however, Chang *et al.* first demonstrated that the development of **L** to **C** actually occurs at $n = 5$ in protonated methanol.^{60,61} A side chain (“tail”) can be further extended from the AA site (which then becomes an AAD site) of the **C** type structure; this structure type is called “cyclic with a tail” (**Ct**), as shown in Fig. 1(d). The **Ct** type can emerge at $n \geq 5$; however, it is practically found at $n \geq 6$ in protonated methanol, because the terminal of the “tail” in **Ct** is an A site, the “tail” moiety can be bound to a position on the ring moiety to form another ring. Then, a “bicyclic” (**bC**) type structure is formed (Fig. 1(e)). This **bC** type is the most compact H-bond network in protonated alcohol clusters. The **bC** type has no free OH group, and this should be a spectral signature of the **bC** type. The **bC** type can be stable in $n \geq 5$; however, its population occurs at $n \geq 7$ in protonated methanol. Further development is limited to expansion of the ring size and attachment of the side chains to the ring moiety. As illustrated in Fig. 1(f), this side chain is terminated by a D site, and it cannot be bound to the ring moiety to form more complicated 3-dimensional networks. Therefore, the **bC** type is the terminal of the topological development of the H-bond networks in protonated alcohols.

For illustration purposes, the minimum electronic energy isomer of each structure type of protonated methanol for $n = 4$ to 8 is shown in Fig. 2.⁵⁶ To search for stable isomers, the first-principles based multi-model method proposed by Nguyen *et al.* was applied.^{141–143} Many structurally distinct isomers were identified using empirical models which were re-optimized using B3LYP/6-31+G(d). The reasonable accuracy of this level of theory for protonated methanol clusters has been confirmed by a comparison with dispersion-corrected density functional theory (DFT) calculations at the ωB97X-D/6-311++G(3df,3pd) level.^{54,144} We finally found 2, 13, 22, 56, and 93 stable isomers for $n = 4, 5, 6, 7$, and 8, respectively.⁵⁶

At the end of this section, we note the structural differences between neutral and protonated methanol clusters. In neutral methanol clusters, $(\text{MeOH})_n$, a linear chain type structure is terminated by A and D site (see Fig. 1(a)). As a result, a cyclic type structure consists only of AD sites, and it cannot have free OH groups. When a side chain is formed in the cyclic type, the side chain is terminated by a D site and cannot be bound to the ring moiety. Therefore, possible H-bond networks of neutral alcohols are restricted to linear or cyclic type, and no more complicated H-bonded networks are formed. Cyclic type structures can be formed at $n \geq 3$. The linear type and cyclic type forms without side chains have been observed for jet-cooled $(\text{MeOH})_n$ with $n = 2$ and $3 \leq n \leq 9$, respectively, by size-selective IR spectroscopy.^{31–36,39,40,42} Linear type structures at $n \geq 3$ have not yet been definitely confirmed for gas phase clusters.^{27–30,41}

III. Temperature dependence of the isomer populations of protonated methanol clusters

The relative population of stable isomers under thermal equilibrium conditions is determined by their free energies.

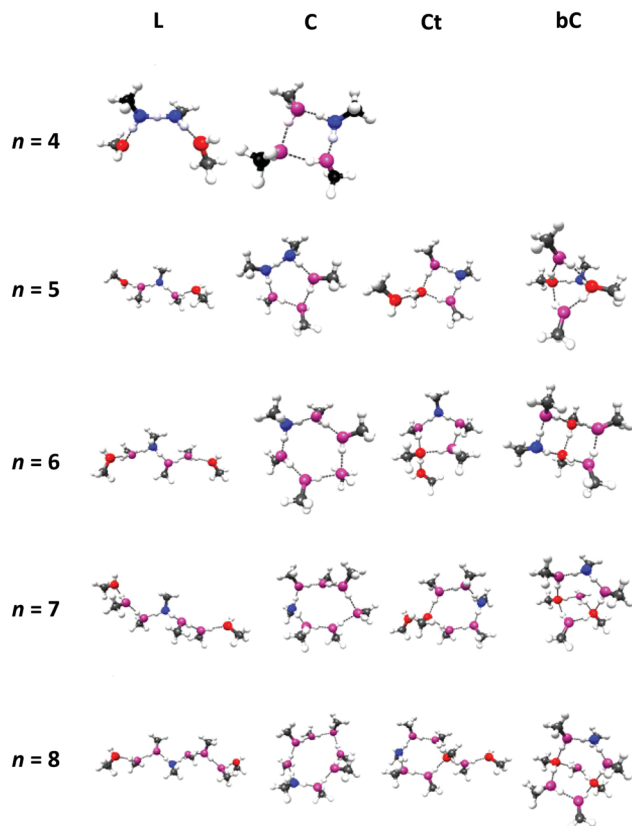


Fig. 2 Structures of the most stable isomers of $\text{H}^+(\text{MeOH})_n$ ($n = 4$ to 8) in each network type. The calculations were performed at the B3LYP/6-31+G(d) level. For easy visualization, the oxygen atoms of the DD and AD sites are shown in blue and pink, respectively. Reproduced from ref. 56 with permission from the PCCP Owner Societies.

Therefore, the relative population depends on temperature through the entropy factor of free energies. In H-bonded clusters, structures with larger numbers of H-bonds tend to have lower electronic energies. These structures, however, tend to be more rigid, and their intermolecular vibrational frequencies are higher than those of more flexible structures with smaller numbers of H-bonds. Therefore, a general trend of temperature dependence of isomer populations is expected; more compact and energetically stable isomers are preferred at low temperature, and entropy promotes populations of isomers with more open and flexible H-bond networks with increasing temperature. Protonated methanol clusters very clearly follow this trend.

The relative population of each isomer type (the sum of the contributions of all the isomers of each structure type) was calculated by the vibrational partition function based on the harmonic approximation. The calculated relative populations of each structure type of $\text{H}^+(\text{MeOH})_n$ at $n = 4$ to 8 are summarized in Fig. 3.⁵⁶ Both C and Ct are grouped together (as C) in Fig. 3 for simplicity. The highest population isomer structures at 50 and 200 K are shown to the left and right of the panel, respectively. We found that the L type dominates the whole temperature range at $n = 4$. For $n = 5$ and 6, the cyclic (both C and Ct) type is energetically more favorable and remains as the

free energy minimum until around 125 K (for $n = 5$) and 160 K (for $n = 6$) before the high energy L type becomes dominant. For $n = 7$ and 8, two structural changes driven by temperature can be seen. At these sizes, the bC type, the terminal morphology of the H-bond networks, is the most energetically stable and survives up to ~ 100 K. Above this temperature, C and Ct are the most abundant groups. At even higher temperatures, the L type finally dominates. As shown in the next section, the present calculations well reproduce the observed spectral changes by inert gas tagging.

IV. IR spectra of protonated methanol clusters and comparison with simulations

IR spectra of the protonated methanol clusters were observed under two different conditions. The first is bare clusters. Because of the large excess energy in the protonation, the (vibrational) temperature of protonated clusters is typically around 200 K even after supersonic jet cooling.⁸³ To select the low internal energy components of protonated clusters, inert gas tagging is frequently employed.^{76–81} When an Ar atom (“tag”) is bound to protonated clusters, only clusters whose internal energies are lower than the binding energy with the Ar atom can hold the tag. Therefore, the effective temperature of the Ar-tagged cluster is much lower than that of the bare protonated cluster; it is typically 50 to 100 K.

Fig. 4 shows the observed IR spectra of (b) Ar-tagged and (d) bare $\text{H}^+(\text{MeOH})_n$ clusters ($n = 4$ to 8) in the OH and CH stretching vibrational region along with the simulated IR spectra at (a) 50 and (c) 200 K.⁵⁶ The upper traces show the full frequency region (2430 to 3840 cm^{-1}), and the lower traces are the expanded plots of the high frequency region (3200 to 3840 cm^{-1}). The temperature dependent spectral simulations are based on the quantum harmonic superposition approximation (QHSA).^{145–147} The harmonic spectra of all the isomers are weighted by their relative populations, shown in Fig. 3, and they are superposed.

In the observed IR spectra, the relatively sharp peaks above 3600 cm^{-1} are assigned to free OH stretch vibrations. The bands below 3600 cm^{-1} are attributed to H-bonded OH stretching vibrations. Some sharp features in the 2800 to 3000 cm^{-1} region are CH stretch bands, and they overlap with the broadened OH stretch bands. With Ar tagging, narrowing of the bandwidths occurs. Moreover, for $n = 5$ to 8, the spectral features clearly change upon tagging. These remarkable spectral changes suggest that the isomer distributions are greatly influenced by tagging.

When the observed spectra of the bare and Ar-tagged clusters are compared with the simulated spectra at 200 and 50 K, respectively, we find that the observed spectral changes upon tagging are reproduced very well by decreasing temperature in the simulations. Although details for each size will be discussed in the following sub-sections, the comparison of the observed and simulated spectra shown in Fig. 4 clearly demonstrates that

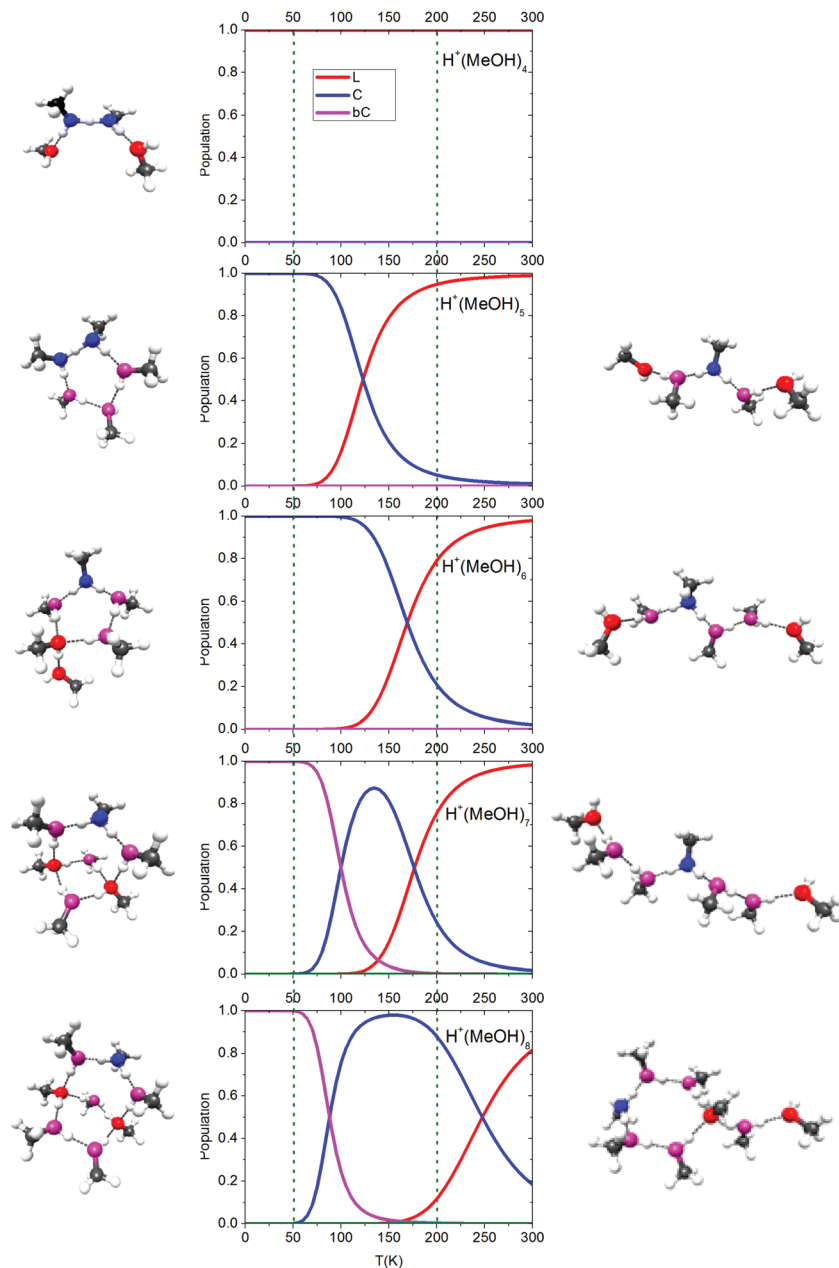


Fig. 3 Temperature dependence of isomer type populations of $\text{H}^+(\text{MeOH})_n$ ($n = 4$ to 8). All the calculations were performed at the B3LYP/6-31+G(d) level. The plots of the **C** type isomers (blue lines) include the populations of the **Ct** type isomers (see text). Except for $n = 4$, the dominant isomer type changes with increasing temperature. At the left and right of the panels, the isomers of the highest populations at 50 and 200 K are displayed, respectively. Reproduced from ref. 56 with permission from the PCCP Owner Societies.

isomer population switching is essential to the spectral changes upon tagging.

$n = 4$ cluster

In the spectrum of the bare cluster of $n = 4$, shown in Fig. 4, a greatly broadened H-bonded OH stretch band is seen below 3500 cm^{-1} , and some features due to CH stretches are overlapped at around 3000 cm^{-1} . A relatively sharp band of the free OH stretches appears at 3673 cm^{-1} . This spectrum is attributed to the **L** type isomer of $n = 4$. In $n = 4$, the spectral changes arising from Ar-tagging are not significant. The spectral features are

essentially retained; however, the peak position of the broadened H-bonded OH band is shifted to a lower frequency by $\sim 200 \text{ cm}^{-1}$ upon tagging.

In $n = 4$, the **L** type isomer is more stable than the **C** type. In addition, the **L** type is more flexible than the **C** type and has lower-frequency intermolecular vibrational modes. Therefore, the **L** type has lower free energy than the **C** type even at high temperature. As expected from this qualitative discussion, the simulation shown in Fig. 3 predicts that the **L** type isomer is exclusive in the entire temperature range. This result supports the small difference between the observed spectra of the bare

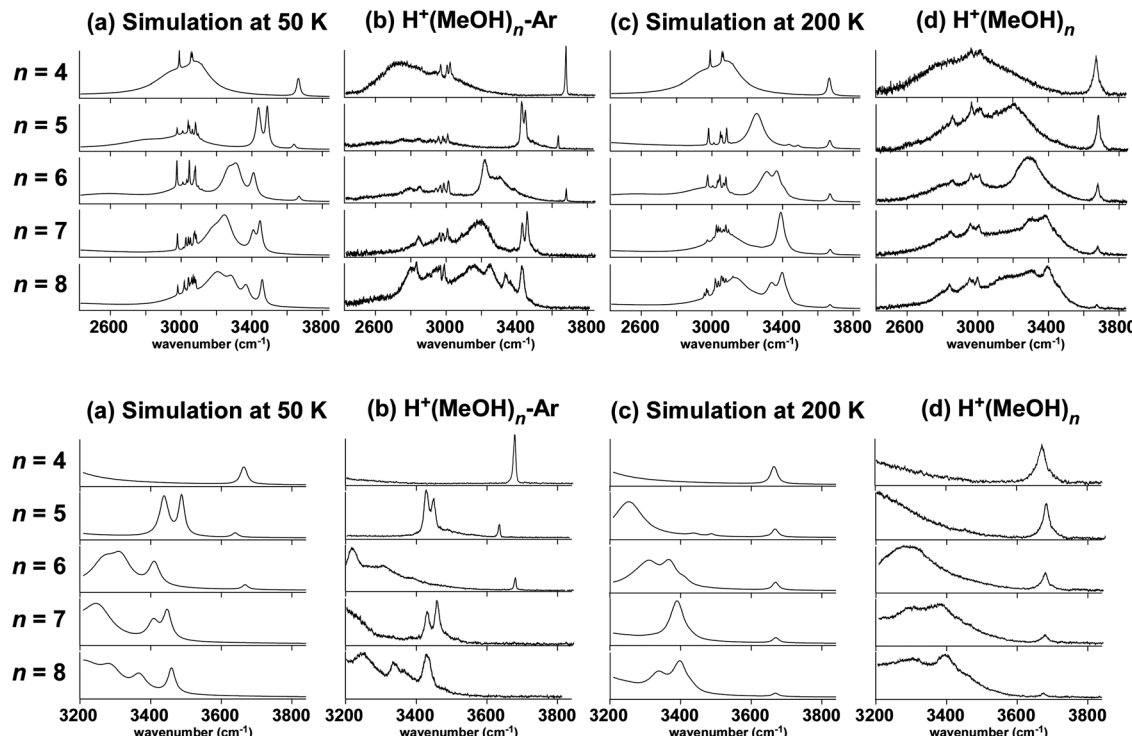


Fig. 4 Comparisons of the observed IR spectra of (b) Ar-tagged and (d) bare $\text{H}^+(\text{MeOH})_n$ clusters ($n = 4$ to 8) with the simulated spectra at (a) 50 K and (c) 200 K, respectively. The upper traces show the full frequency region (2430 to 3840 cm^{-1}), and the lower traces are the expanded plots of the high frequency region (3200 to 3840 cm^{-1}). The spectral simulations were performed at the B3LYP/6-31+G(d) level. The observed spectra of Ar-tagged clusters agree well with the simulated spectra at lower (~ 50 K) temperature, and the observed spectra of the bare clusters resemble the simulated spectra at higher temperature (~ 150 to 200 K). Reproduced from ref. 56 with permission from the PCCP Owner Societies.

and tagged clusters shown in Fig. 4. The remarkable shift of the peak position of the H-bonded OH band with tagging can be attributed to the excitation energy dependence of the predissociation yield in the bare cluster. The assistance of thermal energy is often required for predissociation of H-bonds upon excitation of low frequency bands, while the dissociation yield of the Ar-tagged cluster is practically at unity in the observed region.^{130,148}

$n = 5$ cluster

In the observed spectrum of the bare cluster with $n = 5$, the spectral features are similar to those with $n = 4$. We should specially note that the free OH band position (3676 cm^{-1}) is the same. The spectrum of the bare cluster with $n = 5$ is attributed to the L type isomers. With tagging, the spectrum of the $n = 5$ cluster shows very noticeable changes; two prominent bands are seen at 3643 and $\sim 3450\text{ cm}^{-1}$. These bands are attributed to more stable C type isomers, which are populated by the decrease of the cluster temperature. The free OH band in the C type is from the AA site, and its frequency (3643 cm^{-1}) is slightly lower than that of the L type isomers (3676 cm^{-1}), which arises from the A sites. The characteristic band of the C type isomers at $\sim 3450\text{ cm}^{-1}$ is assigned to the stretching vibration of the OHs bound to the AA site in the H-bonded ring. This is a marker band of H-bonded ring formation in $\text{H}^+(\text{MeOH})_n$.

The spectral changes upon tagging, especially those on the free OH bands, indicate that the cooling of the cluster by

Ar tagging causes 100% switching of the population from the L type to the C type. The isomer population simulation of $n = 5$ is shown in Fig. 3. For $n = 5$, the most stable structure is the C type, and its distribution is predominant at $T \leq \sim 125$ K. However, the L type isomer is more flexible and has lower frequency intermolecular vibrational modes. Therefore, in contrast with the case of $n = 4$, the distribution of the L type isomer increases with increasing temperature because of the entropy factor. At ~ 125 K, the relative distribution is inverted, and at $T \geq \sim 170$ K, the L type isomer becomes dominant. As seen in Fig. 4, the observed spectrum of the bare cluster well agrees with the simulation of $T = 200$ K, which is exclusively attributed to the L type. The finite temperature of the bare cluster is due to the large excess energy from the formation of the protonated cluster. On the other hand, the spectrum of the Ar-tagged cluster is reproduced by the simulation at $T = 50$ K, which is due to the neat C type isomers. The upper limit of the temperature (T_{\max}) of the Ar-tagged cluster estimated by the binding energy with Ar is 56 to 91 K. This T_{\max} evaluation is highly consistent with the observed isomer distribution of the tagged clusters.

We should note that the C type isomers have Zundel type ion cores (the excess proton is shared by two methanol sites), while the L type isomers have Eigen type ion cores (the excess proton is localized on a single methanol site). A proton transfer mechanism associated with the switching between the L and C isomers has been proposed by Chang *et al.*^{60,61} This complete switching

of the isomer population in the $n = 5$ cluster is a good example of the temperature dependence of H-bonded network structures. The temperature dependence of $n = 5$ will be examined in detail later.

$n = 6$ cluster

In the observed spectrum of the bare cluster with $n = 6$, a further shift to higher frequency is seen for the H-bonded OH stretch bands, and a free OH band appears at the same position (3677 cm^{-1}) as that for $n = 4$ and 5. With tagging, in contrast to the case of $n = 5$, the spectral changes appear to be much less remarkable except for the band narrowing. It is worth noting that the free OH stretch band with the Ar tag shows the same frequency (3676 cm^{-1}) as that of the bare cluster. Despite the similar spectral features of the two spectra, the isomer population simulation strongly suggests complete isomer population switching with tagging, similar to the case of $n = 5$, and it accurately reproduces the observed spectra. For $n = 6$, the **Ct** type is the most stable isomer, and its population is dominant at $T \leq \sim 150\text{ K}$. With increasing temperature, a population of **L** isomers occurs because of the entropy factor, and it becomes dominant at $T \geq \sim 200\text{ K}$. As shown in the IR simulation in Fig. 4, the IR spectra of the **Ct** (50 K) and **L** (200 K) type isomers are very similar in both the free and H-bonded OH regions. Here, we note that the free OH of the **Ct** type in its "tail" moiety is an A site; therefore, its stretch frequency is essentially the same as that of the **L** type. This is in contrast with the case of $n = 5$, in which the free OH site in the **C** type is an AA site and its frequency is clearly different from that of an A site in the **L** type.

$n = 7$ and 8

For $n = 7$, the **bC** type, which has the most compact H-bond network, is the most stable. The spectral signature of the **bC** type is the disappearance of the free OH stretch band. While the bare cluster shows a weak free OH band (in the bare cluster, the weakening of the free OH band with increasing n is reasonably explained by the decrease of the number ratio of free OHs relative to H-bonded OHs), it disappears in the Ar-tagged cluster. In addition, strong H-bonded OH bands, which are marker bands of H-bonded ring formation, appear at 3400 to 3500 cm^{-1} with tagging. All these changes suggest that the isomer distribution changes drastically with tagging. The spectral simulation demonstrates that the tagged spectrum is well reproduced by the cold spectrum at $T = 50\text{ K}$, in which the **bC** type is predominant, while the bare cluster agrees with the higher temperature spectra at $T = 200\text{ K}$, which is consistent with the **L** and **Ct** types. Therefore, we observe closing (**bC** formation) of the totally open (**L**) or partially open (**Ct**) H-bond networks with tagging (decreasing temperature).

The $n = 8$ cluster also shows similar results to the $n = 7$ cluster. With tagging, disappearance of the free OH band and appearance of new H-bonded OH bands occur. The simulation for $n = 8$ shows a parallel result to that of $n = 7$. The most stable isomer is the **bC** type, and its population is dominant at low temperatures of $T \leq \sim 70\text{ K}$. Distribution of the **Ct** and **L** types occurs with increasing temperature. The observed spectrum

with the Ar tag is accurately reproduced by the simulation at $T = 50\text{ K}$, and the spectrum of the bare cluster agrees with that at $T = 200\text{ K}$.

V. Comparison with other systems

The systematic study through this size range ($n = 4$ to 8) clearly demonstrates a general trend of the size and temperature dependence of the microscopic H-bond networks of protonated methanol. The open (unfolded) networks are formed in the bare cluster because of the excess energy upon protonation and cluster formation. In other words, the bare cluster is warm ($T = \sim 150$ to 200 K) under the present ion source conditions, and entropy is the dominant factor to determine the preferred network structure. With tagging, the temperature of the cluster is limited by the weak intermolecular bond with the tag ($T \leq \sim 70\text{ K}$); the H-bond network changes to the more compact (folded) forms, which are stabilized by greater numbers of H-bonds and are preferred by the enthalpy factor.

Comparison with water and neutral methanol clusters

A remarkable feature of protonated methanol clusters is that complete switching between the populated isomer types occurs with tagging (vibrational cooling) in the size range of $n = 5$ to 8. This contrasts with the case of protonated water clusters $\text{H}^+(\text{H}_2\text{O})_n$ in the same size region.^{50,51,83,98,100,101,103–105,123} Although Ar tagging and/or temperature control by an ion trap cell have been applied to $\text{H}^+(\text{H}_2\text{O})_n$, the magnitude of the isomer population change is much smaller ($n = 6$ and 7) or almost negligible ($n = 5$ and 8). This difference can be attributed to the close competition between the multiple isomers and/or the high relative energies of the flexible (chain type) isomers in protonated water clusters. Both these effects originate from the strong preference for multiple H-bond coordination of water. The striking contrast between protonated methanol and water demonstrates the advantage of protonated methanol as a benchmark to study the temperature dependence of H-bond networks.

The temperature dependence of H-bond networks in neutral water clusters ($\text{H}_2\text{O})_n$ has also been studied for $n = 3$, 4, and 9 by changing the conditions of the supersonic jet cluster source.^{71,72,74,75} For $n = 3$ and 4, changes from the stable cyclic structure to the linear structure have been suggested with increasing temperature; however, the linear structure is transient at these sizes.^{74,75,149} Moreover, the temperature of the warm cluster has not been decisively determined. At $n = 9$, clear transformation from compact cube-like structures to multiple open structures with increasing temperature from 69 to 186 K has been observed by the crossed molecular beam technique.^{71,72,127} Similar to the case of protonated water, the multiple cluster structures simultaneously compete at this size; this prevents detailed analysis of the warm spectrum, which is greatly broadened. Moreover, the crossed molecular beam experiment is highly complicated and advanced; thus, it is not being pursued at present.

The temperature dependence of H-bond networks of neutral methanol clusters (MeOH)_n has also been studied by the crossed molecular beam experiment.⁷³ However, this study has been limited to the boat-chair isomer conversion of cyclic (MeOH)₆. To simulate a liquid, the quantum cluster equilibrium approach (interacting cluster model) has been applied to methanol, and it has been shown that an ensemble of (small) cyclic clusters simulates the macro properties of liquid methanol better than those of linear and cyclic clusters with side chains.^{20,150} We should note that while the L structure is almost dominant at 200 K in protonated methanol, dominance of the cyclic structure is suggested for neutral methanol even at around 300 K. For $n = 3$ and 4, the lowest energy isomers are cyclic in neutral methanol but linear in protonated clusters. This is because the protonated site strongly prefers non-deformed (straight) H-bonds in protonated methanol, while a higher number of H-bonds is advantageous for neutral methanol even if each H-bond is somewhat deformed. This larger relative stability of the cyclic isomer in neutral clusters is the reason for its preference in liquid methanol at ~ 300 K.

An entropy-driven population of more flexible networks with increasing temperature is commonly seen in statistical cluster model calculations of various alcohols and water.^{20,121–123,127,151,152}

Implications for H-bond networks of methanolated ions

As demonstrated above, the development of the H-bond networks of protonated methanol can be readily understood by topological considerations based on the coordination properties of methanol. This success encouraged us to apply the same concept to prediction of the H-bonded network structures of methanolated ions, $\text{X}^\pm(\text{MeOH})_n$ (X^+ = metal cations, X^- = halide anions). As a model of ion solvation, the structures of methanolated ions have been extensively studied both for cations and anions.^{107–120} In the 1st solvation shell, several methanol molecules independently solvate the central ion. However, the solvation motifs are different for anions and cations. In the case of anions, methanol donates its proton to the anion and acts like a D site in the H-bond networks.^{107–112} On the other hand, the lone pair of methanol is attached to the cation, and methanol acts like an A site.^{113–120} The main focus of these studies, however, is the determination of the coordination number of the ion, which can be evaluated by the cluster size at the appearance of the 2nd solvation shell. Therefore, solvation structures (H-bond networks) after completion of the 1st shell have been rarely discussed. The application of topological considerations to methanolated ions predicts very different H-bond networks for anions and cations after completion of the 1st shell.

Fig. 5 displays schematics of the solvation structures of methanolated ions. Except for the directions of the methanol molecules, the 1st solvation structures of anions and cations are similar. However, the H-bonded networks after completion of the 1st shell are largely influenced by the H-bond direction of the 1st shell molecules. In anions, the H-bonded chains are terminated by D sites (Fig. 5(a)). These chains have no free OH groups and cannot be bound to each other. Therefore,

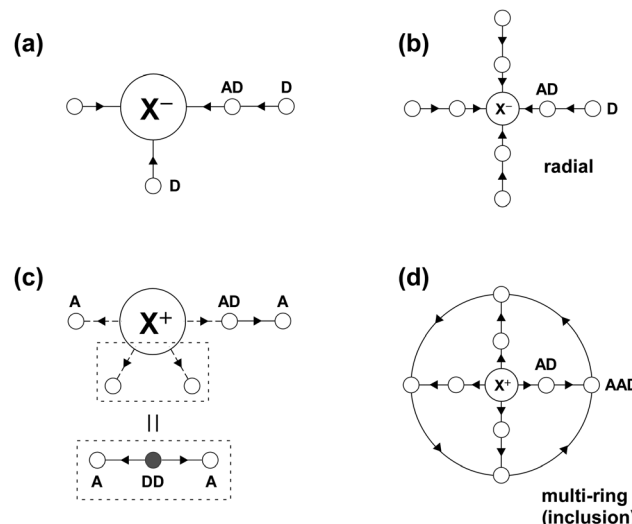


Fig. 5 Schematics of the expected hydrogen bond network structures of methanolated ions, $\text{X}^\pm(\text{MeOH})_n$. The same symbols as Fig. 1 are employed. (a) Initial stage of the solvation of an anion. (b) Radial chain structure formed in a fully solvated anion. (c) Initial stage of the solvation of a cation. (d) Multi-ring (inclusion) structure formed in a fully solvated cation.

the network development with increasing cluster size is limited only to the extension of the chain length. ‘‘Radial’’ chain structures, schematically shown in Fig. 5(b), are concluded for fully solvated anions. On the other hand, the 1st shell molecules in cations are A sites. If we pick up a pair of neighboring molecules in the 1st shell, its H-bond coordination properties are equivalent to that of an L type isomer of protonated methanol (Fig. 5(c)). Therefore, the local H-bond network of this pair can develop into C, Ct, and bC types, as in protonated methanol. Moreover, these local units can be bound to each other (instead of the formation of bC); this a conformation results in a closed H-bond network, as shown in Fig. 5(d). A similar H-bond network structure, called a ‘‘multi-ring’’ or ‘‘inclusion’’ structure, can be constructed for $\text{H}_3\text{O}^+(\text{MeOH})_n$, and its actual formation was recently confirmed by IR spectroscopy and theoretical computations of $\text{H}^+(\text{MeOH})_n(\text{H}_2\text{O})_1$.^{153,154} For methanolated ions, H-bonded network structures in the 2nd and 3rd shells have not yet been closely examined, except for some trials of theoretical modeling.^{112,113,115} Experimental confirmation of H-bond networks in large methanolated ions is future work of great interest.

VI. Stepwise change of the internal energy of clusters upon tagging

As seen in the previous sections, the isomer distribution of a cluster can greatly change with temperature. Therefore, to fully understand the nature of the hydrogen bond structures of the cluster, not only its most stable structure but also the temperature dependence of its preferred structures is very important. In the case of protonated clusters, because of the large excess energy of the protonation, the produced clusters are usually

warm (~ 200 K) even after supersonic jet expansion cooling. Therefore, the internal energy restriction by Ar-tagging, employed in the previous section, is very useful to observe preferred isomers under low temperature conditions. However, to experimentally confirm the temperature dependence profile of the isomer distribution, two temperature points (corresponding to the bare and Ar-tagged clusters) are not necessarily sufficient, and variable change of temperature is highly necessary.

Because inert gas tagging provides a cutoff for the internal energy according to the binding energy with the tag, it is possible to change the internal energy distribution of the protonated cluster stepwise by systematic changes of the tag species from strongly bound to weakly bound. We should note that the internal energy distribution of such a tagged cluster is not necessarily under thermal equilibrium. However, if suppression of the high energy population by tagging is a good approximation of a decrease in temperature, it is possible to explore the temperature dependence profile of the isomer distribution of a cluster. Thus, we applied IR spectroscopy to $\text{H}^+(\text{MeOH})_5$ with various tag species to test whether tagged clusters can enable monitoring of the isomer distribution in a wide range of temperatures.⁵⁷

The observed IR spectra of $\text{H}^+(\text{MeOH})_5\text{-X}$ clusters (X = (a) bare, (b) C_6H_6 , (c) C_2H_2 , (d) CS_2 , (e) CO_2 , (f) CO, and (g) Ar) in the OH and CH stretching vibrational region are shown in Fig. 6. In the spectra of the bare and Ar-tagged clusters, the clusters were produced by a different ion source from that in Fig. 4 to unify the ion source with that of the other tagged clusters. The tagged species are ordered according to the estimated binding energies between the tags and the bare cluster.

The spectra of the bare and Ar-tagged clusters are uniquely attributed to the **L** and **C** type isomers, respectively, as shown in the previous section. The observed spectra of the CO, CO_2 , and CS_2 -tagged clusters show essentially the same spectral features as those of the Ar-tagged cluster. Therefore, these clusters are attributed to the **C** type. On the other hand, the spectrum of the C_6H_6 -tagged cluster is similar to that of the bare cluster; this means that the C_6H_6 -tagged cluster is **L** type, in which C_6H_6 is π -hydrogen-bonded to the methanol moiety. The spectrum of the C_2H_2 -tagged cluster appears to be unique. This spectrum can be readily interpreted as a combination of **L** and **C** type isomers with an additional band due to the free acetylenic CH stretch at 3270 cm^{-1} (see Fig. S1 in the ESI† for detailed assignments of the bands). Therefore, the **C** and **L** types coexist under C_2H_2 -tagging conditions.

The observed spectra of the $\text{H}^+(\text{MeOH})_5\text{-X}$ tagged clusters show that the major isomer type changes from the **C** type to the **L** type with increasing binding energy with the tag species (*i.e.*, the internal energy of the cluster). From the Ar to CS_2 tags, the **C** type is dominant. The two isomer types coexist with the C_2H_2 tag, and the dominant isomer type changes to the **L** type with the C_6H_6 tag. These stepwise changes of the isomer distribution follow the isomer distribution changes with increasing temperature, as shown in Fig. 3. The coexistence of the two isomer types in the C_2H_2 -tagged cluster can be regarded as the “phase change point” in the $n = 5$ cluster.

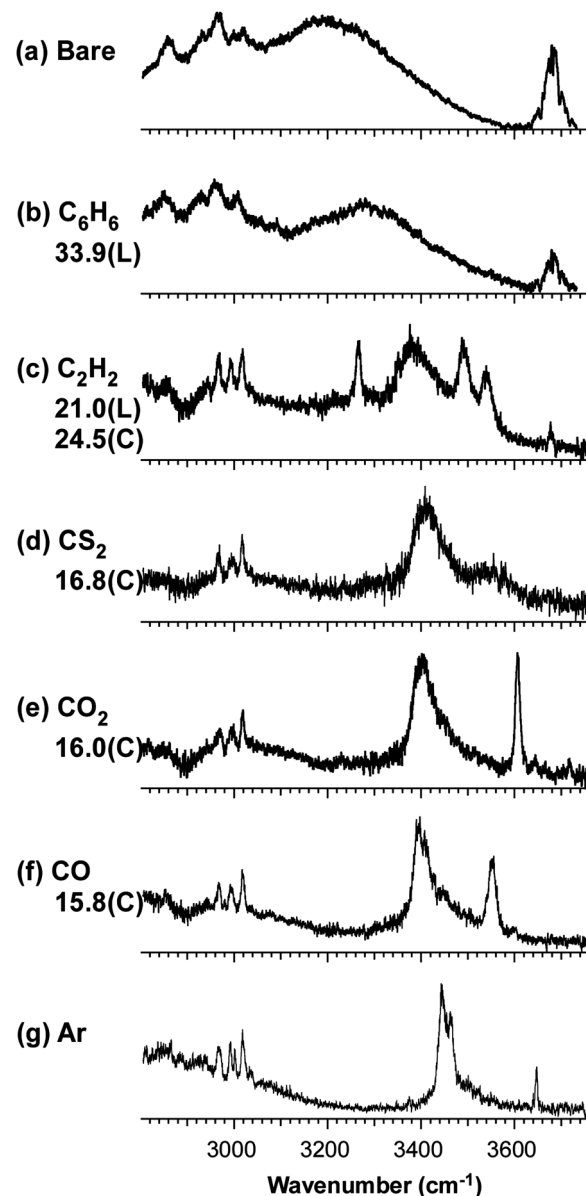


Fig. 6 Observed IR spectra of $\text{H}^+(\text{MeOH})_5\text{-X}$ clusters (X = (a) bare, (b) C_6H_6 , (c) C_2H_2 , (d) CS_2 , (e) CO_2 , (f) CO, and (g) Ar) in the OH and CH stretching vibrational region. The binding energies with the X tag species (in kJ mol^{-1}) are also shown in the figure. The binding energy was estimated at the $\omega\text{B97X-D/6-311++G(3df,3pd)}$ level, and the assumed structure type of the bare cluster is indicated in parentheses (L or C). Adapted with permission from ref. 57. Copyright 2016 American Chemical Society.

The tag variation method was also tested for $\text{H}^+(\text{MeOH})_7$. As seen in the previous section, the **bC** type is the most stable structure at $n = 7$, and the **L** type is dominant at high temperature. These low and high temperature limit cases are observed in the Ar-tagged and bare clusters, respectively. The temperature dependence of the isomer population in Fig. 3 predicts that the **C** (**Ct**) type becomes dominant in the intermediate temperature range.⁵⁴ Fig. 7 shows the observed spectra of $\text{H}^+(\text{MeOH})_7\text{-X}$. The spectrum of the CS -tagged cluster is essentially the same as that of the Ar-tagged cluster and is attributed to the **bC** type isomer. The spectrum of the C_6H_6 -tagged cluster

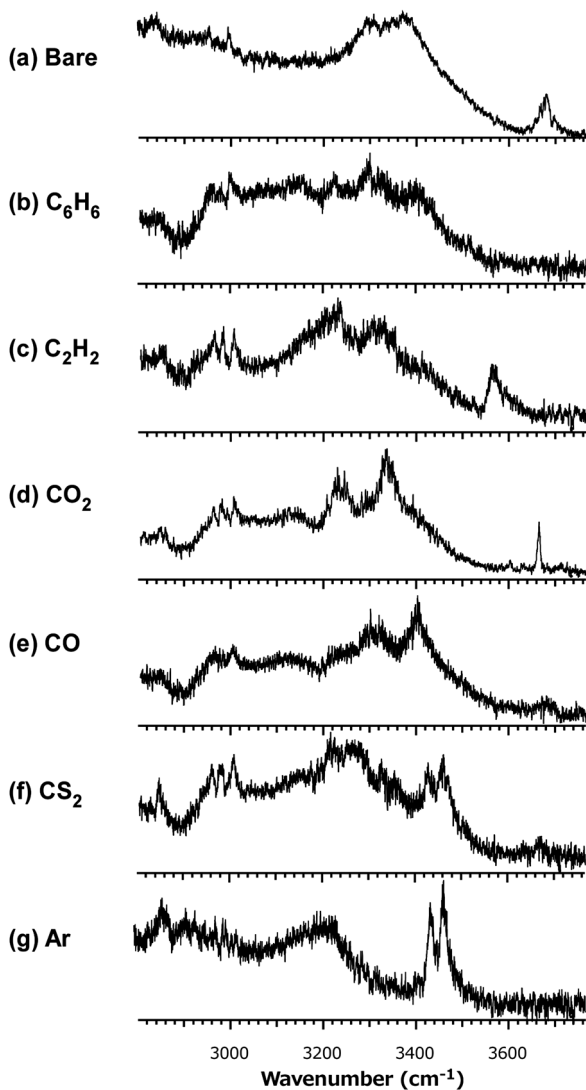


Fig. 7 Observed IR spectra of $\text{H}^+(\text{MeOH})_7\text{-X}$ clusters ($\text{X} = \text{(a)} \text{ bare}, \text{(b)} \text{ C}_6\text{H}_6, \text{(c)} \text{ C}_2\text{H}_2, \text{(d)} \text{ CO}_2, \text{(e)} \text{ CO}, \text{(f)} \text{ CS}_2, \text{ and (g)} \text{ Ar}$) in the OH and CH stretching vibrational region.

is similar to that of the bare cluster of the **L** type isomer. On the other hand, the spectra of the CO, CO₂, and C₂H₂ tagged clusters are similar to each other but are different from the spectra of both the **bC** and **L** type isomers, and they are consistent with the spectra of the **Ct** isomers (a comparison between the observed spectra and simulations of some **Ct** isomers is shown in Fig. S2 and S3 in the ESI[†]). Although reliable evaluation of the binding energy is practically difficult at $n = 7$ because so many isomer structures are possible at this size, it seems reasonable that the intermediate binding energies of the CO, CO₂, and C₂H₂ tags fall between those of the Ar and C₆H₆ tags. The tag dependence of the $n = 7$ cluster demonstrates that a dominant isomer in the intermediate temperature range can be observed by proper choice of the tag species.

The recent development of cryogenic ion trap techniques enables arbitrary control of the temperature of ionic (or, in many cases, protonated) hydrogen-bonded clusters.^{82–96,105,130,131}

We should emphasize that the use of a cryogenic ion trap is an ideal approach to precisely explore the temperature dependence of the isomer distribution of ionic clusters. However, we also note that IR spectroscopy of ionic clusters is usually based on dissociation spectroscopy. To maintain a constant dissociation yield irrespective of the excitation vibrational frequency, inert gas tagging is frequently required for IR spectroscopy of cryogenic ions.¹³⁰ However, after tagging is employed, the binding energy between the cluster and tag also determines the upper limit of vibrational energy of the tagged cluster to avoid thermal evaporation of the tag. Therefore, to observe higher temperatures, a more strongly bound tag is actually required. This means that even cryogenic ion trap IR spectroscopy can be equivalent to the present tag variation method in such a case.

VII. Larger clusters of protonated methanol

The topological development of the H-bond networks of protonated methanol clusters is terminated by the **bC** type formation, as discussed in the above sections. More complicated network structures are forbidden by the restriction of the H-bond coordination properties of methanol. Therefore, even at larger sizes ($n \geq \sim 10$), these H-bonded structures can be categorized into the **L**, **C**, **Ct**, and **bC** types. When the cluster size increases while the H-bond network type is retained, expansion of the ring or chain size simply occurs and results only in an increase of the number of AD sites. An alternative process associated with cluster size increase is the formation of side chains which are terminated by D sites. A number of patterns (branching point and chain length) can be considered for such side chain formations; this suggests the entropic advantage of side chain formation at relatively high temperature.

To probe the dominant process in large protonated methanol clusters, we performed IR spectroscopy of size-selected $\text{H}^+(\text{MeOH})_n$ in the size region of $n = 10$ to 50.⁵⁵ Because of the weak signal intensity of the large clusters, we only observed the spectra of the bare clusters. The observed IR spectra are shown in Fig. 8. The H-bonded OH stretch band centered at 3300 cm^{-1} appears, and the CH stretch bands partially overlap with the low frequency tail of the OH band. No clear free OH stretch band appears in the spectra. Narrowing of the spectral features is seen with increasing cluster size, and the spectral features converge in the size range of $n \geq \sim 30$. This is attributed to the evaporation cooling and increase of the heat capacity in larger clusters and also to the dilution of the contribution of the strongly H-bonded sites around the protonated ion core.

Here, we examine the contribution of side chains in large clusters. We note that side chain formation is associated with the formation of AAD and D sites at the ends of the chains, while the expansion of the ring or chain only causes an increase of the AD sites. Therefore, the ratio of the AD/AAD (or AD/D) sites should be a measure of the relative weight of the side chains in the H-bond network. DFT simulations demonstrate that the H-bonded OH stretch in an AD site of methanol

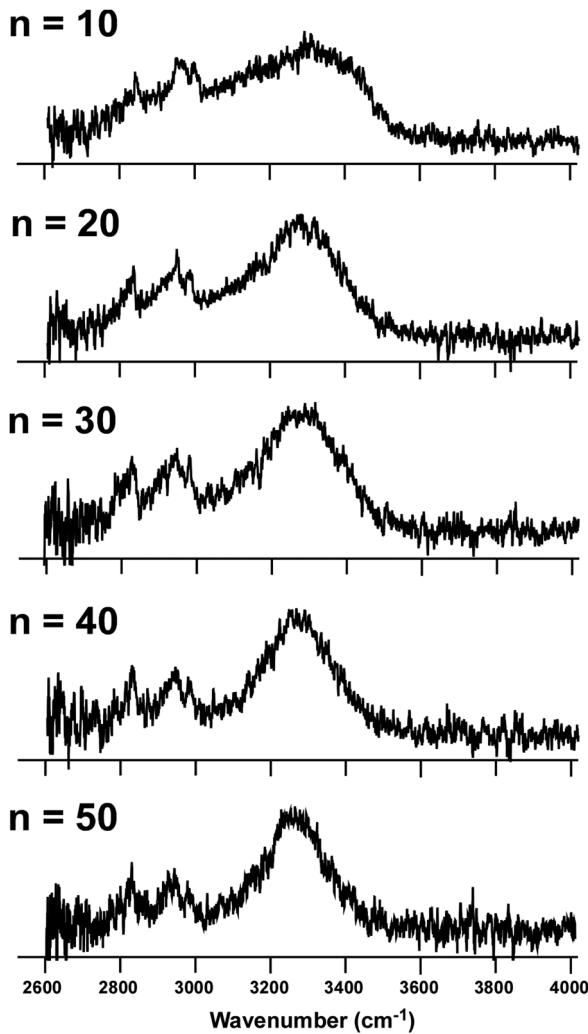


Fig. 8 IR spectra of $\text{H}^+(\text{MeOH})_n$ in the size region of $n = 10$ to 50. Reproduced from ref. 55 with permission from the PCCP Owner Societies.

generally appears in the 3200 to 3400 cm^{-1} region.⁵⁵ On the other hand, the OH stretch of an AAD site is located at around 3100 cm^{-1} , which is clearly low-frequency shifted from that of the AD site. This low-frequency shift can be readily explained in terms of the H-bond cooperativity. Because of the acceptance of two protons, the H atom of the AAD site is highly polarized; thus, its H-bond is stronger. In addition, the OH stretch band of the terminal D site of a side chain is shifted to the high frequency region ($\sim 3500\text{ cm}^{-1}$). This is also due to the (decrease of) cooperativity.

In order to quantitatively estimate the contribution of side chain formation (AAD and D sites) in large methanol clusters, we examined the measured IR spectrum of $\text{H}^+(\text{MeOH})_{50}$, which is the largest size we measured.⁵⁵ We decomposed the bands in the observed spectrum by multiple Gaussian peak fitting, as frequently performed in band analyses of condensed phase spectra. Fig. 9 shows the results of the decomposition by (a) three components (two CH stretches and the AD component of the OH stretches) and (b) five components (two CH stretches and the AAD, AD, and D components of the OH stretches).

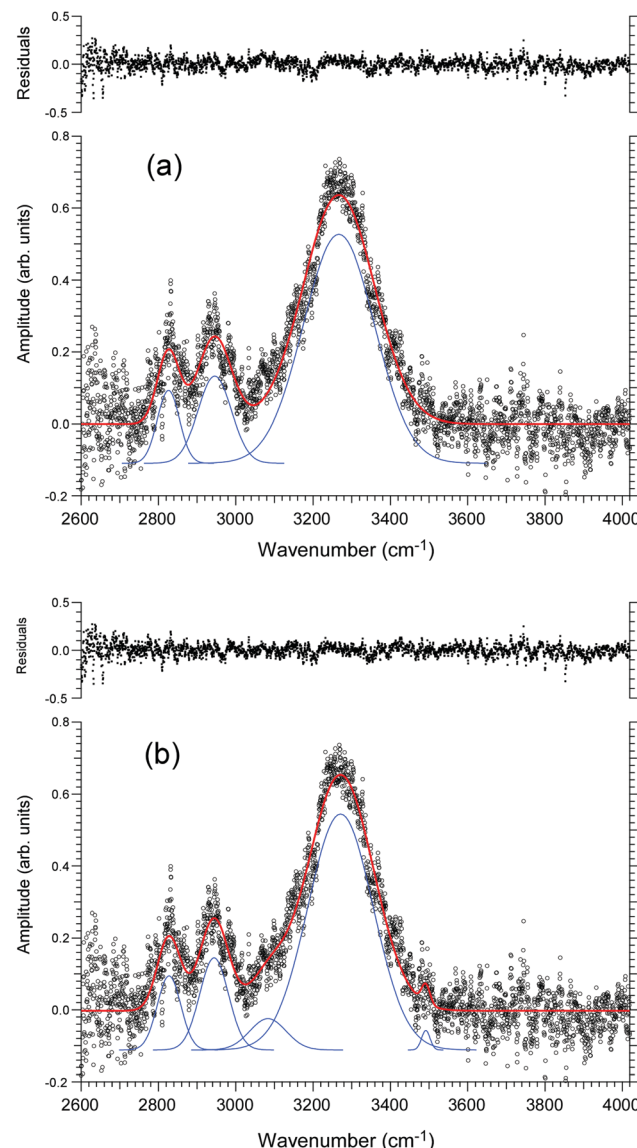


Fig. 9 Band decomposition of the observed IR spectrum of $\text{H}^+(\text{MeOH})_{50}$. (a) Three-component decomposition. (b) Five-component decomposition. The upper panel in each figure shows the residual of the fitting. Reproduced from ref. 55 with permission from the PCCP Owner Societies.

The five-component decomposition results in slightly better fitting than the three-component decomposition ($\sim 5\%$ decrease of residual error). This comparison suggests that there should be some contribution from the AAD and D sites. However, the weights of the AAD and D components relative to the AD component are estimated to be only $\sim 7\%$ and $\sim 1\%$, respectively. If we roughly suppose that all OH stretch oscillators have the same transition intensity, the observed relative weight of the AAD site ($\sim 7\%$) corresponds to 3 to 4 AAD sites in $\text{H}^+(\text{MeOH})_{50}$.

If we assume the **Ct** or **bC** types for the clusters because of the larger heat capacities and corresponding lower temperatures of the larger clusters, they involve 1 or 2 AAD sites even without side chains. In addition, the contribution of at least two charge-enhanced H-bonded OH oscillators (methanol molecules next to the ion core)

is also expected in the same frequency region as the AAD site. Therefore, at most, only one or two side chains can be formed in $\text{H}^+(\text{MeOH})_{50}$. The present results demonstrate that methanol prefers networks essentially composed only of AD sites and that branching of the networks (AAD/D site formation) is almost negligible, at least in networks with 50 molecules.

Here, we note the role of dispersion in large clusters. The predominance of AD sites has been also concluded for larger neutral methanol (MeOH_n) clusters; therefore, folded single ring structures have been supposed for these large clusters.^{37,38} Recent theoretical studies, however, have demonstrated that stacked double ring structures in which two independent H-bonded rings are bound by dispersion compete with single ring structures at $n \geq \sim 15$.^{45,47} Because these two structure types have the same number of H-bonds (no free OH in either type), optimization of dispersion is essential to determine their relative energies. Although no theoretical studies have been performed for protonated methanol clusters in the large size region, these dispersion-bound type structures can be competitive also in protonated methanol clusters once the bC type is formed (no free OH) and the cluster size is large enough to form a counterpart to be bound by dispersion.

Convergence of the cluster structure into the bulk structure with increasing cluster size is an important subject in recent cluster gas phase studies.^{48–50,72,155,156} Here, we compare the observed IR spectrum of $\text{H}^+(\text{MeOH})_{50}$ with the previously reported bulk spectra of methanol in the CH and OH stretching vibrational regions. We have confirmed that the IR spectra of large $\text{H}^+(\text{MeOH})_n$ clusters are almost identical to those of neutral (MeOH_n) in the size range of $n \geq \sim 30$, and the influence of the excess proton on the spectral features in the observed region is practically negligible in this size region.⁵⁵ Bulk spectra of (a) liquid (300 K), (b) vitreous solid (93 K), and (c) crystal (93 K, α phase) methanol reported by Falk and Whalley are reproduced in Fig. 10 with (d) the spectrum of $\text{H}^+(\text{MeOH})_{50}$.³ The OH stretch band peak position of the cluster is quite similar to those of the vitreous solid and crystal, although the size of the network in the cluster is still much smaller than that in the solid phase. This strongly contrasts with the case of water, in which the convergence of the band position of the cluster (into that of the ice spectrum) occurs in a much larger size region ($n = \sim 500$).^{48–50,72,155} As discussed above, the essentially one-dimensional H-bond network of methanol restricts the effective area of the cooperative enhancement between H-bonds; this causes the fast convergence of the OH stretch frequency with increasing cluster size. On the other hand, there is a remarkable difference between the spectra of liquid methanol and of the cluster. The OH frequency of the liquid is clearly higher than that of the cluster. This difference suggests that the major H-bond network size in the liquid is much smaller than $n = \sim 10$. This notion agrees with the predictions of theoretical simulations.^{5–26} Another factor which contributes to the higher OH frequency in the liquid is its higher temperature. Although the precise temperature of the cluster is not known, it is expected to be lower than that of the much smaller cluster ($n \leq 8$) produced by the same ion source because of the evaporation cooling and the larger

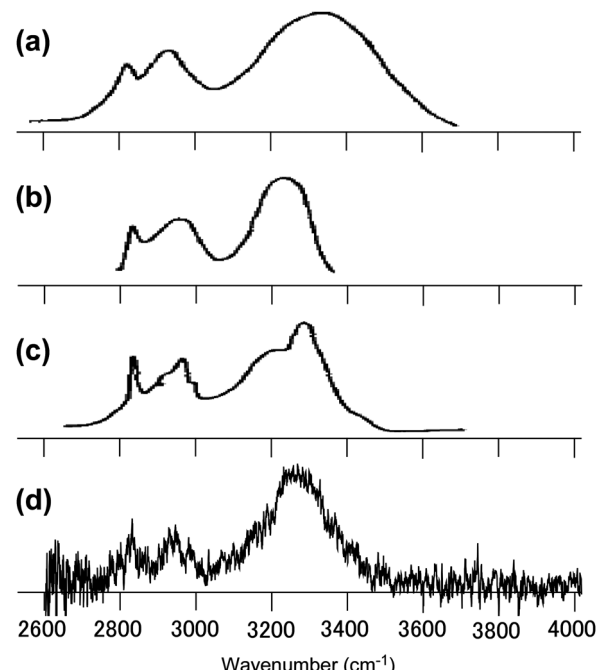


Fig. 10 Comparison of the IR spectra of methanol in condensed phases with that of $\text{H}^+(\text{MeOH})_{50}$. (a) Liquid at 300 K, (b) vitreous solid at 93 K, (c) crystal at 93 K, and (d) $\text{H}^+(\text{MeOH})_{50}$. (a–c) Reprinted with permission from ref. 3. Copyright [1961], American Institute of Physics. (d) Reproduced from ref. 55 with permission from the PCCP Owner Societies.

heat capacity of the larger cluster. Therefore, the temperature of $\text{H}^+(\text{MeOH})_{50}$ should be lower than ~ 200 K, which is much lower than the room temperature (300 K) of liquid methanol. Excitation of intermolecular vibrations should weaken the H-bond strength; this can also cause a partial shift of the OH band in liquid methanol to a higher frequency. To provide a definite conclusion, elucidation of the wide range temperature dependence of size-selected neutral methanol clusters is greatly needed.

VIII. H-Bonded network structures of protonated normal-chain alcohol clusters

As noted in the Introduction, alcohols contain an alkyl group, and the magnitude of dispersion between the alkyl groups increases with increasing cluster size. To examine the influence of dispersion on H-bonded network structures, we observed the IR spectra of protonated clusters of four normal-chain alcohols H^+X_n ($\text{X} = \text{ethanol (EtOH)}, \text{1-propanol (1-PrOH)}, \text{1-butanol (1-BuOH)}, \text{or 1-pentanol (1-PeOH)}}$) in the size range of $n = 4$ to 7. To observe the temperature dependence of the H-bonded structures, both the spectra of the bare and Ar-tagged clusters were measured. The spectra of the $n = 4$ to 7 clusters in the OH and CH stretch region are shown in Fig. 11–14, respectively, with those of $\text{H}^+(\text{MeOH})_n$, which were analyzed in the previous sections.

The spectra of the $n = 4$ clusters are summarized in Fig. 11. For the bare clusters (spectra (b) in the figure), the CH stretch band intensity at around 3000 cm^{-1} largely increases with

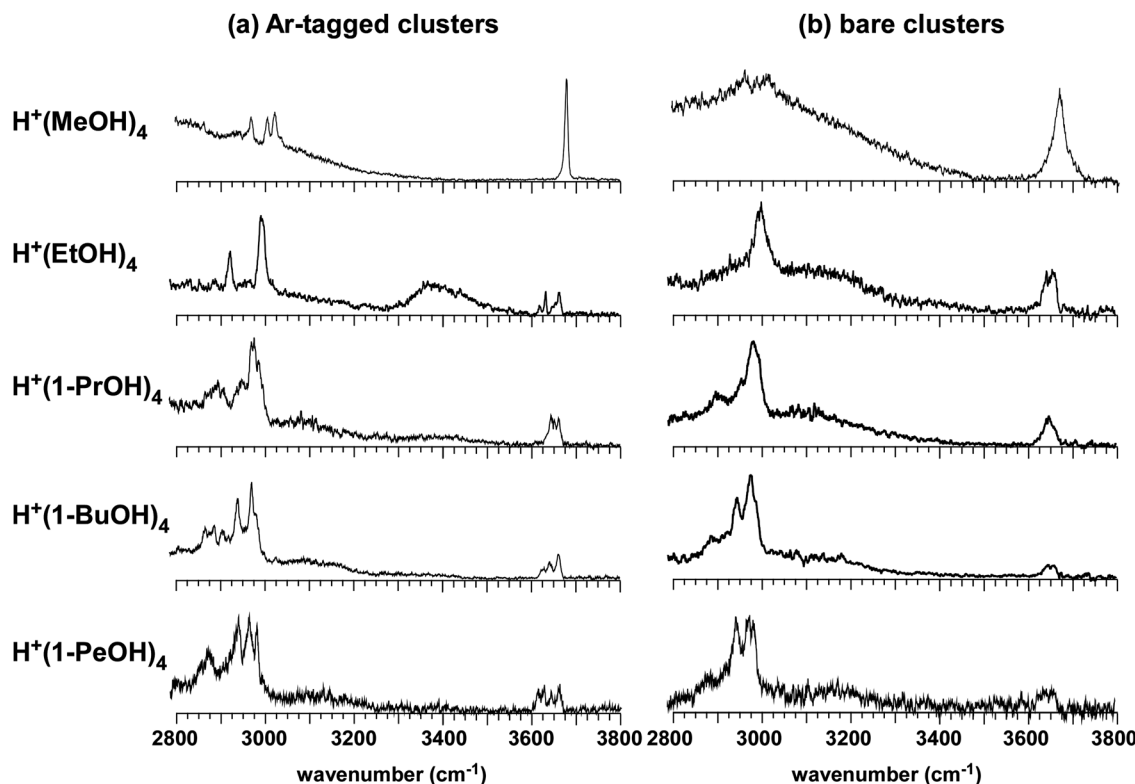


Fig. 11 IR spectra of $\text{H}^+(\text{alcohol})_4$ clusters in the OH and CH stretch region. (a) Ar-tagged clusters. (b) Bare clusters. EtOH, 1-PrOH, 1-BuOH, and 1-PeOH are ethanol, 1-propanol, 1-butanol, and 1-pentanol, respectively.

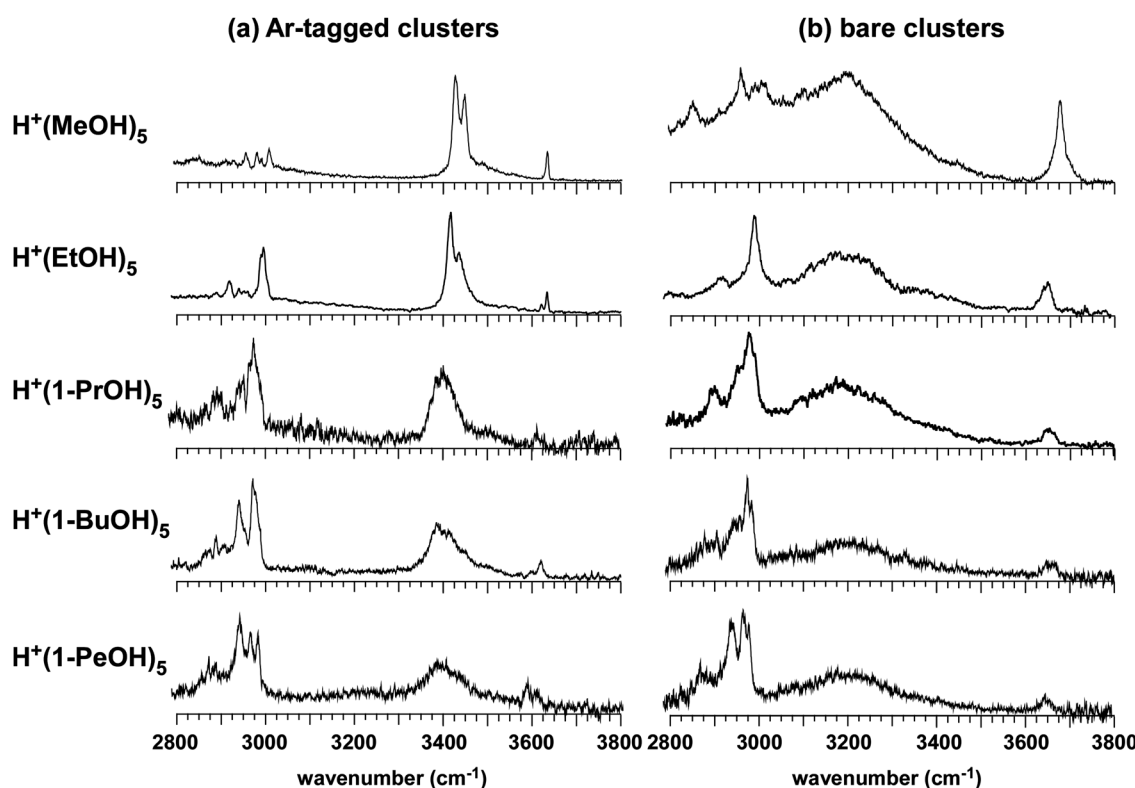


Fig. 12 IR spectra of $\text{H}^+(\text{alcohol})_5$ clusters in the OH and CH stretch region. (a) Ar-tagged clusters. (b) Bare clusters.

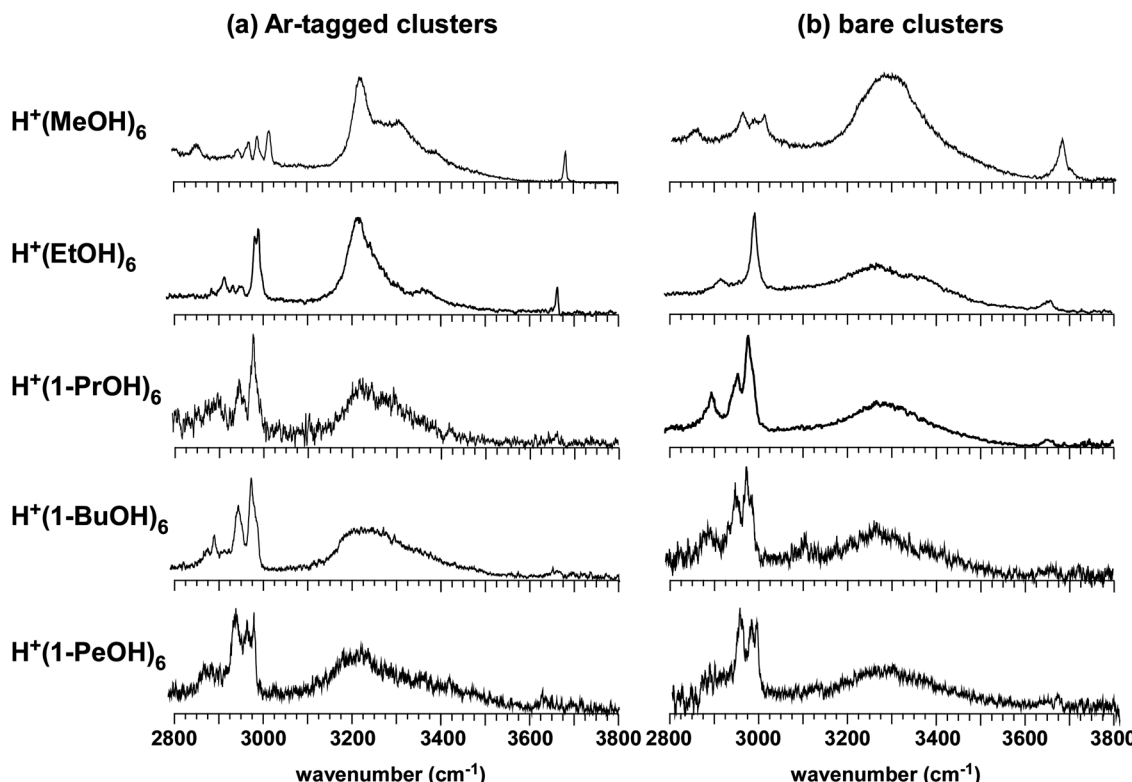


Fig. 13 IR spectra of $\text{H}^+(\text{alcohol})_6$ clusters in the OH and CH stretch region. (a) Ar-tagged clusters. (b) Bare clusters.

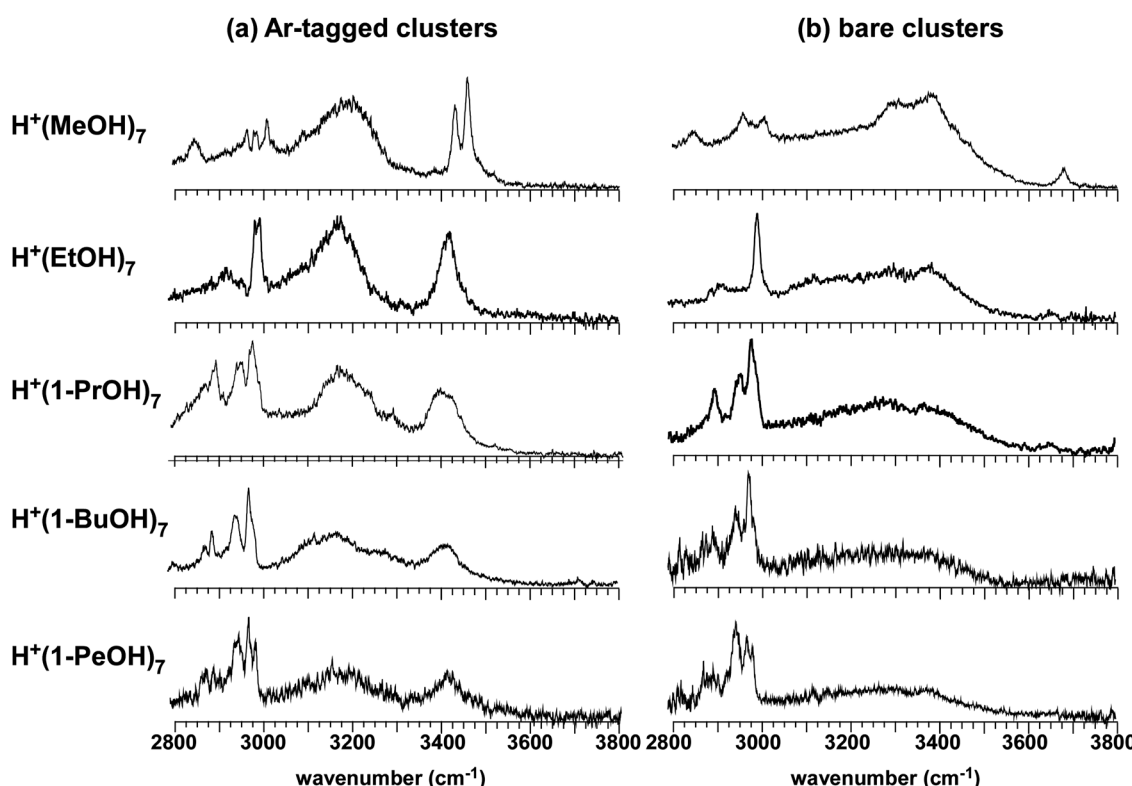


Fig. 14 IR spectra of $\text{H}^+(\text{alcohol})_7$ clusters in the OH and CH stretch region. (a) Ar-tagged clusters. (b) Bare clusters.

increasing alkyl chain length. However, the OH stretch region is almost the same in all the spectra if we normalize the band intensities with the free OH band. The band above 3600 cm^{-1} is assigned to the free OH stretch of the terminal A site, and a very broadened absorption below $\sim 3400\text{ cm}^{-1}$ is attributed to the H-bonded OH stretch. A weak low-frequency shift trend of the free OH stretch band is seen with extension of the alkyl chain. In $n = 4$ clusters, only the L and C types are practically possible H-bond network structures (the Ct type requires a three-membered ring containing a protonated site; such a ring has never been observed). The free OH stretch of the A site demonstrates that the bare clusters uniquely have L type structures. For $\text{H}^+(\text{EtOH})_4$, the same conclusion has been reported by Socà and Dopfer, although their measurement was limited above 3400 cm^{-1} .^{62,63}

In $\text{H}^+(\text{MeOH})_4$, the L type structure is the most stable structure. Therefore, no isomer switching occurs with Ar tagging (lowering temperature), and the spectral feature of the tagged cluster is essentially same as that of the bare cluster. However, in $\text{H}^+(\text{EtOH})_4$, remarkable spectral changes are seen with Ar tagging. The spectrum of $\text{H}^+(\text{EtOH})_4\text{-Ar}$ shows another free OH band on the low frequency side. Moreover, an H-bonded OH band clearly appears at around 3400 cm^{-1} . Socà and Dopfer also observed the appearance of these new bands upon N₂-tagging; however, they assumed only the L type structure in their spectral analysis, and the origin of these bands has not been identified.⁶³ As seen in the spectrum of $\text{H}^+(\text{MeOH})_5\text{-Ar}$ (Fig. 4), the free OH stretch of an AA site is slightly red-shifted from that of an A site, and the H-bonded OH band at 3400 cm^{-1} is attributed to OH bound to the AA site. These bands are marker bands of the C type structure. Therefore, the spectrum of $\text{H}^+(\text{EtOH})_4\text{-Ar}$ shows the coexistence of the L and C types. We measured also the spectrum of $\text{H}^+(\text{EtOH})_4\text{-Ar}_2$ (see Fig. S4 in ESI†); we found that the two bands of the C type are dominant in the spectrum with Ar₂ tagging, while the bands of the L type are largely suppressed. These features of the tagged spectra suggest that the C type structure is the most stable structure in $\text{H}^+(\text{EtOH})_4$. In the bare cluster, the population of the L type isomer is driven by entropy; however, the decrease of temperature due to tagging induces a population change to the more stable C type isomer. The Ar₂-tagged cluster is colder than the Ar-tagged cluster, and the population of C type is almost exclusive. The lower temperature of the Ar₂-tagged cluster can be rationalized if we suppose that the two Ar atoms are separately bound to the cluster and that the binding energy of the second Ar atom is lower than that of the first Ar atom because the strongest binding site is already occupied by the first Ar atom.

When we carefully examine the spectrum of $\text{H}^+(\text{1-PrOH})_4\text{-Ar}$, we find that the changes upon Ar-tagging, *i.e.* the appearance of the bands of the C type structure, also occur in 1-PrOH. Ar₂-tagging also results in further enhancement of these bands (see Fig. S4 in ESI†). However, the spectral changes are much weaker than for EtOH; this suggests that the L type isomer is the most stable isomer in $\text{H}^+(\text{1-PrOH})_4$ and that the C type population will be very small. In the spectra of $\text{H}^+(\text{1-BuOH})_4$

and $\text{H}^+(\text{1-PeOH})_4$, no clear change of the free OH band is seen upon Ar and Ar₂-tagging. Moreover, the H-bonded OH band around 3400 cm^{-1} is totally absent in the tagged spectra. Therefore, in these two species, the L type is the most stable structure at $n = 4$.

The observed isomer population changes with tagging do not indicate perfect switching in $\text{H}^+(\text{EtOH})_4$ and $\text{H}^+(\text{1-PrOH})_4$. This suggests that the energy difference of the L and C types is very small, and competition between the isomers can occur at very low temperature.

To theoretically assess the influence of the flexibility of the longer alkyl chain in EtOH, we carried out a systematic exploration to search for the conformational isomers of both the L and C types of $\text{H}^+(\text{EtOH})_4$. The details of our searching scheme can be found in the ESI.† These initial structures were first subjected to geometry optimization using three different DFT methods: (1) B3LYP/6-31+G*, (2) ωB97X-D/6-311+G(2d,p), and (3) B3LYP/6-31+G* with D3 correction. Hessians of the optimized structures were checked to ensure that they were local minima and to correct their zero-point energies. The relative energies of two sets of structurally distinct C and L forms are shown in the top panels of Fig. 15. Although the number of initial structures is the same, after screening out duplicates, there were more structurally distinct L forms than C forms. The three DFT functionals had different tendencies regarding the relative energies of conformers of the L and C types of $\text{H}^+(\text{EtOH})_4$. B3LYP/6-31+G* indicates that the L type isomers are more stable. When dispersion is included, ωB97X-D/6-311+G(2d,p) concludes that the majority of conformers in both types have nearly the same energy. B3LYP/6-31+G*+D3 shows the opposite trend from B3LYP/6-31+G*. However, these three functionals all show the same spectral features for these two types of conformers: (1) the H-bonded OH band at $\sim 3400\text{ cm}^{-1}$ is the marker band of the C type, (2) the diffused band at $\sim 3000\text{ cm}^{-1}$ can be seen for the L type, and (3) the free O-H stretching modes in the L type are higher in frequency than their counterparts in the C type (see Fig. S8 in the ESI†).

To include the difference in the number of distinct isomers and vibrational free energy corrections, we evaluated the thermal properties at elevated temperature by engaging QHSA. The temperature dependence of the populations of the two types of hydrogen bond network is summarized in the lower panels in Fig. 15. With B3LYP/6-31+G*, the L form dominates the whole temperature range. When dispersion is included, both ωB97X-D/6-311+G(2d,p) and B3LYP/6-31+G*+D3 predict a temperature range in which both the L and C types can co-exist. However, these two DFT functionals showed very different trends in the low-temperature region. In either case, at low temperature (below 100 K), the IR spectrum is dominated by a single type of conformer; this conclusion is inconsistent with the experimental observation of Ar-tagged $\text{H}^+(\text{EtOH})_4$. Because we performed an extensive conformation search (see ESI†), we conclude that (1) none of these three functionals can quantitatively reproduce the experimental spectra and (2) due to the sensitive dependence on conformation with respect to thermal energy, this cluster is an ideal system to benchmark the accuracy of DFT calculations.^{157–159}

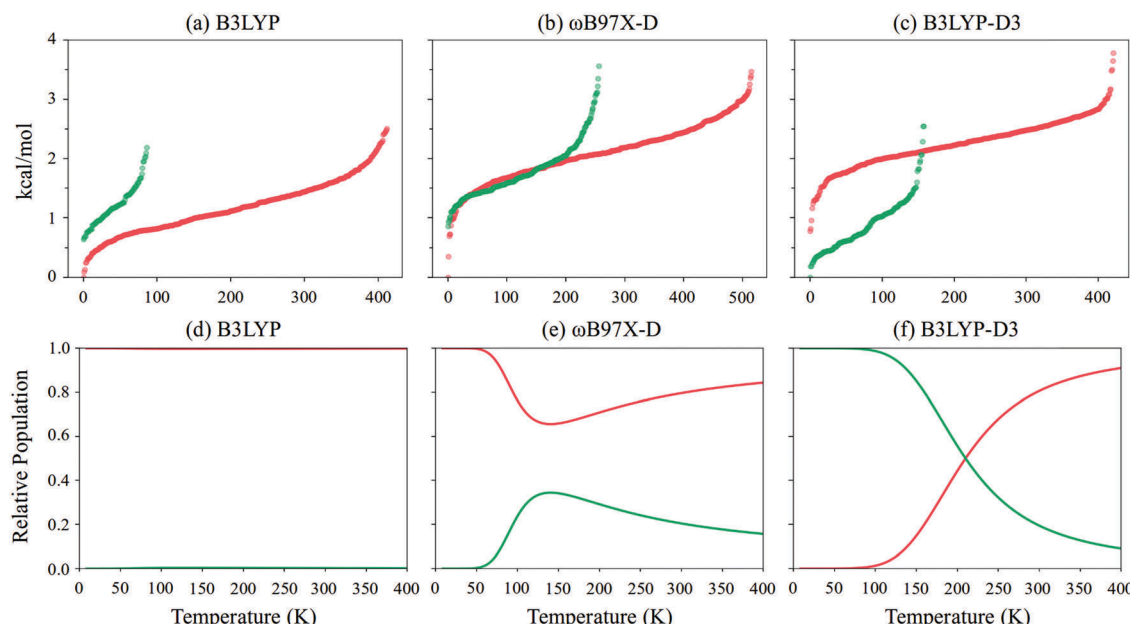


Fig. 15 Top panels: Relative energies of structurally distinct $\text{H}^+(\text{EtOH})_4$ conformers with **C** (green) and **L** (red) types of hydrogen bonds using the (a) B3LYP/6-31+G*, (b) ω B97X-D/6-311+G(2d,p), and (c) B3LYP/6-31+G*+D3 methods. The abscissa is the numbering of the isomers. The populations of the two types of conformers (**C** type = green and **L** type = red) are shown in the bottom panels.

In contrast with $n = 4$, the spectra of the protonated normal-chain alcohol clusters of $n = 5$ to 7, shown in Fig. 12–14, are quite similar to those of corresponding $\text{H}^+(\text{MeOH})_n$ species, irrespective of the tagging. As general trends, slight red-shifts of the OH stretch bands and enhancements of the CH stretch band intensities are seen with extension of the alkyl chains (we should note that the latter results in suppression of the relative OH stretch band intensities). However, all the spectra of the protonated normal-chain alcohol clusters of the same size show common spectral features in the OH stretch region, which are characteristic of their H-bonded network type. Moreover, the spectral changes upon Ar-tagging were also common to all the clusters. We also measured the spectra of the Ar₂-tagged clusters, as shown in Fig. S5–S7 of the ESI.[†] However, the spectra of the Ar₂-tagged clusters are identical to those of the Ar-tagged clusters in $n = 5$ to 7. In $n = 5$, the bare cluster shows a single free OH stretch band at the high frequency end of the spectra, while the free OH band of the Ar-tagged cluster is red-shifted by 20 to 30 cm^{-1} and a clear band appears at $\sim 3400 \text{ cm}^{-1}$. The former is the spectral signature of an A site, and the latter two are that of an AA site. Therefore, the **C** type is the most stable H-bonded network of $n = 5$, and complete switching of the isomer population to the **L** type occurs with increasing temperature in all the short-chain alcohols. The spectral signature of $n = 6$ is less prominent. However, all the clusters show similar features. We should note that the free OH band frequency does not change upon tagging. This is consistent with the case of $\text{H}^+(\text{MeOH})_6$, in which the **Ct** type is the most stable and the population switch to the **L** type occurs at high temperature. On the other hand, the spectral signature of the $n = 7$ clusters is clear; a weak free OH band is seen in the bare clusters, but it completely disappears upon tagging.

An intense H-bonded OH band also appears at $\sim 3400 \text{ cm}^{-1}$ upon tagging. Therefore, the **bC** type, which does not have a free OH, is formed in the tagged clusters at low temperature, and it transforms to the **L** or **Ct** type in the bare clusters at high temperature.

It is worthwhile to note another general trend seen in the observed IR spectra of the protonated normal-chain alcohol clusters. The bandwidth of the OH stretch bands becomes larger with increasing alkyl chain length. The band broadening trend is also clearly observed in the spectra of the Ar- and Ar₂-tagged clusters. Therefore, thermal effects may not be essential to the band broadening with extension of the alkyl chain. If the conformation of the alkyl chain slightly influences the hydrogen bond strength and causes a small shift of the OH band, the greater number of conformational isomers in longer alkyl chain alcohols reasonably explains the band broadening trend.¹⁶⁰ This suggests that the influence of the alkyl conformation on the hydrogen bonds is not totally negligible, although the influence is not strong enough to greatly change the framework of the hydrogen bond networks, at least with these normal alkyl chains.

In the protonated normal-chain alcohols, the $n = 4$ clusters appear to be somewhat exceptional. The clusters of EtOH and 1-PrOH show a delicate balance between the H-bonds and van der Waals interactions (including steric hindrance, *i.e.*, exchange repulsion) and the energy order of the **C** and **L** types changes along with the alkyl chain length. All the other sized clusters, however, have the same H-bond network structure trends as $\text{H}^+(\text{MeOH})_n$. It is especially interesting that the two longest normal-chain alcohols in the present study, 1-BuOH and 1-PeOH, follow exactly the same trends as MeOH in the entire observed size range. The present results demonstrate

that the normal alkyl chain of alcohols hardly interferes with the H-bond network structure. This is consistent with the similarity between the crystalline structures of the normal short chain alcohols.^{135,136,161,162} The magnitude of dispersion among alkyl chains should increase with increasing chain length. However, the normal alkyl chain is very flexible, and the present results reveal that optimization of the normal-alkyl chain conformation is possible without large deformation of the H-bond network structure, even in the most compact **bC** type. In neutral alcohols, it has been proved that $(\text{cyclohexanol})_n$ ($n = 3$ to 6) forms cyclic structures similar to $(\text{MeOH})_n$.^{139,140} For protonated alcohol clusters, the present study is the first systematic research on the competition between H-bond and van der Waals interactions.

IX. Summary and future tasks

In this perspective, we reviewed our previous work on protonated methanol clusters, $\text{H}^+(\text{MeOH})_n$; we also presented the latest structure analyses of other protonated short normal-chain alcohol clusters. Finally, we summarize the present results and future tasks they have inspired.

The most important characteristic of the hydrogen bond network structures of protonated alcohols is their simplicity, which is in sharp contrast with the complicated networks of water. Protonated alcohols can be ideal model systems to examine the properties of hydrogen bond networks. Their hydrogen bond network structures can be categorized into only four types. The protonated methanol clusters are a prototype of protonated alcohols and can serve as a reference to examine other short normal-chain alcohols. The IR spectra of protonated methanol clusters clearly demonstrate the development process of the network structures with cluster size. In the size range of $n = 4$ to 7, more complicated network types are formed with increasing cluster size. The topological development of the network reaches its terminal at $n = 7$, with the formation of the **bC** type. The validity of this simple topological consideration is proved for the structural analyses of protonated methanol. The application of a similar approach to methanolated ions suggests very different solvation motifs for anions and cations. The solvation structures of methanolated ions after the completion of the 1st shell have not yet been fully studied. The present prediction by the topological consideration should be tested by a combination of IR spectroscopy and a theoretical isomer search.

The IR spectra of the larger protonated methanol clusters suggest that further size increase results only in expansion of the hydrogen bonded ring size or chain length, and side chain formation is almost negligible. Moreover, convergence of the cluster spectra to the spectrum of solid methanol is seen at much smaller sizes than in the case of water. Comparison with the bulk spectra also suggests that the hydrogen bond ring size of liquid methanol is smaller than ~ 10 . However, the effects of temperature on the spectra remain equivocal, and studies of the wide range temperature dependence of size-selected

neutral clusters are also highly necessary to provide a definite conclusion.

The IR spectra of the $n = 5$ to 8 clusters of protonated methanol show remarkable temperature (internal vibrational energy) dependence, and the theoretical analyses based on QHSA demonstrate that the complete switching of the network type occurs upon temperature elevation, which corresponds to the phase change in the bulk. Stepwise changes of the internal energy of the cluster are achieved by inert gas tagging. This temperature control by inert gas tagging is simple but provides a rough approximation. The cryogenic ion trap technique can be applied for rigorous temperature control of protonated (ionic) species. The exact temperature dependence of protonated methanol clusters as a prototype of hydrogen bond networks should be examined. In the theoretical approach, QHSA is a very powerful and useful approximation to handle an ensemble of a large number of conformers. However, vibrations of H-bonds are known to be highly anharmonic; therefore, the influence of anharmonicity on the isomer population may be important.^{163–165} However, further confirmation requires a more accurate estimate of the vibrational density of state using methods beyond harmonic approximation. Isotope effects on the temperature dependence are also an interesting future topic of study. Isotopic H/D substitution of OH and CH changes the zero point energy level and vibrational state density; also, it may result in changes in the isomer distributions and their temperature dependence. Theoretical prediction of these isotope effects has been reported, although experimental confirmation has not yet been performed.¹⁵⁰

The hydrogen bond structures of the protonated clusters of the longer normal-chain alcohols are also examined by comparison of their IR spectra with those of the protonated methanol clusters. It is shown that the short normal alkyl chain does not interfere greatly with the formation of the most stable hydrogen bond network structures. Interference between hydrogen bonds and bulky alkyl groups has been suggested in theoretical calculations of branched alkyl alcohol clusters,^{151,152} such a system should be explored by spectroscopy and an extensive theoretical isomer search. Two exception cases in the present study, $(\text{H}^+(\text{EtOH})_4$ and $\text{H}^+(\text{1-PrOH})_4$), serve as good model systems for further theoretical and computational studies to benchmark the accuracy of quantum chemistry methods to balance the subtle competition between hydrogen bonding and dispersion interactions. Such a benchmark system is highly necessary to evaluate rapidly developing density functional theories.^{157–159}

Conflicts of interest

There are no conflicts to declare.

Acknowledgements

A. F. and J.-L. K. acknowledge the essential contribution of the following collaborators: Prof. Naohiko Mikami, Satoko Enomoto,

Mitsuhiko Miyazaki, Tomohiro Kobayashi, Ryoko Yamazaki, Yuta Suzuki, Kenta Mizuse, Ryunosuke Shishido, and Michael C. H. Wu.

References

- 1 J. McMurry, *Organic Chemistry*, Brooks/Cole, Belmont, 7th edn, 2008.
- 2 G. S. Parks, *J. Am. Chem. Soc.*, 1925, **47**, 338–345.
- 3 M. Falk and E. Whalley, *J. Chem. Phys.*, 1961, **34**, 1554–1568.
- 4 A. H. Narten and A. Habenschuss, *J. Chem. Phys.*, 1984, **80**, 3387–3391.
- 5 G. Pálinskás, E. Hawlicka and K. Heinzinger, *J. Phys. Chem.*, 1987, **91**, 4334–4341.
- 6 P. A. Giguère and M. Pigeon-Gosselin, *J. Solution Chem.*, 1988, **17**, 1007–1014.
- 7 M. Matsumoto and K. E. Gubbins, *J. Chem. Phys.*, 1990, **93**, 1981–1994.
- 8 S. Sarkar and R. N. Joarder, *J. Chem. Phys.*, 1993, **99**, 2032–2039.
- 9 J. E. Bertie, S. L. Zhang, H. H. Eysel, S. Baluja and M. K. Ahmed, *Appl. Spectrosc.*, 1993, **47**, 1100–1114.
- 10 J. E. Bertie and S. L. Zhang, *J. Mol. Struct.*, 1997, **413–414**, 333–363.
- 11 E. Tsuchida, Y. Kanada and M. Tsukada, *Chem. Phys. Lett.*, 1999, **311**, 236–240.
- 12 O. Kristiansson, *J. Mol. Struct.*, 1999, **477**, 105–111.
- 13 T. Yamaguchi, K. Hidaka and A. K. Soper, *Mol. Phys.*, 1999, **96**, 1159–1168.
- 14 H. Torii, *J. Phys. Chem. A*, 1999, **103**, 2843–2850.
- 15 B. H. Torrie, O. S. Binbrek, M. Strauss and I. P. Swainsonz, *J. Solid State Chem.*, 2002, **166**, 415–420.
- 16 J. A. Morrone and M. E. Tuckerman, *J. Chem. Phys.*, 2002, **117**, 4403–4413.
- 17 M. Pagliai, G. Cardini, R. Righini and V. Schettino, *J. Chem. Phys.*, 2003, **119**, 6655–6662.
- 18 J.-H. Guo, Y. Luo, A. Augustsson, S. Kashtanov, J.-E. Rubensson, D. K. Shuh, H. Ågren and J. Nordgren, *Phys. Rev. Lett.*, 2003, **91**, 157401.
- 19 J.-W. Handgraaf, E. J. Meijer and M.-P. Gaigeot, *J. Chem. Phys.*, 2004, **121**, 10111–10119.
- 20 R. Ludwig, *ChemPhysChem*, 2005, **6**, 1369–1375.
- 21 H. B. Yu, D. P. Geerke, H. Y. Liu and W. E. van Gunsteren, *J. Comput. Chem.*, 2006, **27**, 1494–1504.
- 22 R. Sharma, C. Chakravarty and E. Milotti, *J. Phys. Chem. B*, 2008, **112**, 9071–9078.
- 23 Ó. Gálvez, B. Maté, B. Martín-Llorente, V. J. Herrero and R. Escribano, *J. Phys. Chem.*, 2009, **113**, 3321–3329.
- 24 M. J. McGrath, I.-F. W. Kuo and J. I. Siepmann, *Phys. Chem. Chem. Phys.*, 2011, **13**, 19943–19950.
- 25 T. Ishiyama, V. V. Sokolov and A. Morita, *J. Chem. Phys.*, 2011, **134**, 024509.
- 26 P. Gomez-Alvarez, L. Romani and D. Gonzalez-Salgado, *J. Chem. Phys.*, 2013, **138**, 044509.
- 27 R. G. Inskeep, J. M. Kelliher, P. E. McMahon and B. G. Somers, *J. Chem. Phys.*, 1958, **28**, 1033–1036.
- 28 A. J. Barnes, H. E. Hallam and D. Jones, *Proc. R. Soc. London, Ser. A*, 1973, **335**, 97–111.
- 29 M. A. Hussein and D. J. Mille, *J. Chem. Soc., Faraday Trans.*, 1976, **72**, 693–699.
- 30 J. R. Dixon, W. O. George, M. H. Hossain, R. Lewis and M. Price, *J. Chem. Soc., Faraday Trans.*, 1997, **93**, 3611–3618.
- 31 R. N. Pribble, F. C. Hagemeister and T. S. Zwier, *J. Chem. Phys.*, 1997, **106**, 2145–2157.
- 32 R. A. Provencal, J. B. Paul, K. Roth, C. Chapo, R. N. Casas, R. J. Saykally, G. S. Tschumper and H. F. Schaefer III, *J. Chem. Phys.*, 1999, **110**, 4258–4267.
- 33 U. Buck, J.-G. Siebers and R. J. Wheatley, *J. Chem. Phys.*, 1998, **108**, 20–32.
- 34 U. Buck and F. Huisken, *Chem. Rev.*, 2000, **100**, 3863–3890.
- 35 A. K. Sum and S. I. Sandler, *J. Phys. Chem. A*, 2000, **104**, 1121–1129.
- 36 H. B. Fu, Y. J. Hu and E. R. Bernstein, *J. Chem. Phys.*, 2006, **124**, 024302–1–9.
- 37 S. Boyd and R. J. Boyd, *J. Chem. Theory Comput.*, 2007, **3**, 54–61.
- 38 M. M. Pires and V. F. DeTuri, *J. Chem. Theory Comput.*, 2007, **3**, 1073–1082.
- 39 R. W. Larsen, P. Zielke and M. A. Suhm, *J. Chem. Phys.*, 2007, **126**, 194307.
- 40 M. A. Suhm, *Adv. Chem. Phys.*, 2009, **142**, 1–57.
- 41 I. Doroshenko, V. Pogorelov, V. Sablinskas and V. Balevicius, *J. Mol. Liq.*, 2010, **157**, 142–145.
- 42 H.-L. Han, C. Camacho, H. A. Witek and Y.-P. Lee, *J. Chem. Phys.*, 2011, **134**, 144309–1–11.
- 43 R. M. Forck, C. C. Pradzynski, S. Wolff, M. Ončák, P. Slavíček and T. Zeuch, *Phys. Chem. Chem. Phys.*, 2012, **14**, 3004–3016.
- 44 M. Umer and K. Leonhard, *J. Phys. Chem. A*, 2013, **117**, 1569–1582.
- 45 S. Kazachenko, S. Bulusu and A. J. Thakkar, *J. Chem. Phys.*, 2013, **138**, 224303.
- 46 Y. Nishimura, Y.-P. Lee, S. Irle and H. A. Witek, *J. Chem. Phys.*, 2014, **141**, 094303–1–11.
- 47 P. J. Hsu, K.-L. Ho, S.-H. Lin and J.-L. Kuo, *Phys. Chem. Chem. Phys.*, 2017, **19**, 544–556.
- 48 V. Buch, S. Bauerecker, J. P. Devlin, U. Buck and J. K. Kazimirski, *Int. Rev. Phys. Chem.*, 2004, **23**, 375–433.
- 49 R. Ludwig, *Angew. Chem., Int. Ed.*, 2001, **40**, 1808–1827.
- 50 A. Fujii and K. Mizuse, *Int. Rev. Phys. Chem.*, 2013, **32**, 266–307.
- 51 J. A. Fournier, C. T. Wolke, M. A. Johnson, T. T. Odbadrakh, K. D. Jordan, S. M. Kathmann and S. S. Xantheas, *J. Phys. Chem. A*, 2015, **119**, 9425–9440.
- 52 A. Fujii, S. Enomoto, M. Miyazaki and N. Mikami, *J. Phys. Chem. A*, 2005, **109**, 138–141.
- 53 J.-L. Kuo, A. Fujii and N. Mikami, *J. Phys. Chem. A*, 2007, **111**, 9438–9445.

- 54 T. Hamashima, Y. C. Li, M. C. H. Wu, K. Mizuse, T. Kobayashi, A. Fujii and J.-L. Kuo, *J. Phys. Chem. A*, 2013, **117**, 101–107.
- 55 T. Kobayashi, R. Shishido, K. Mizuse, A. Fujii and J.-L. Kuo, *Phys. Chem. Chem. Phys.*, 2013, **15**, 9523–9530.
- 56 Y.-C. Li, T. Hamashima, R. Yamazaki, T. Kobayashi, Y. Suzuki, K. Mizuse, A. Fujii and J.-L. Kuo, *Phys. Chem. Chem. Phys.*, 2015, **17**, 22042–22053.
- 57 T. Shimamori, J.-L. Kuo and A. Fujii, *J. Phys. Chem. A*, 2016, **120**, 9203–9208.
- 58 X. Zhang, X. Yang and A. W. Castleman Jr, *Chem. Phys. Lett.*, 1991, **185**, 298–302.
- 59 M. Meot-Ner, *J. Am. Chem. Soc.*, 1992, **114**, 3312–3322.
- 60 H.-C. Chang, J.-C. Jiang, S. H. Lin, Y. T. Lee and H.-C. Chang, *J. Phys. Chem. A*, 1999, **103**, 2941–2944.
- 61 H.-C. Chang, J.-C. Jiang, H.-C. Chang, L. R. Wang and Y. T. Lee, *Isr. J. Chem.*, 1999, **39**, 231–243.
- 62 N. Solcà and O. Dopfer, *J. Am. Chem. Soc.*, 2004, **126**, 9520–9521.
- 63 N. Solcà and O. Dopfer, *J. Phys. Chem. A*, 2005, **109**, 6174–6186.
- 64 Y. J. Hu, F. B. Fu and E. R. Bernstein, *J. Chem. Phys.*, 2006, **125**, 154306.
- 65 T. D. Fridgen, L. Macaleese, T. B. McMahon, J. Lemaire and P. Maitre, *Phys. Chem. Chem. Phys.*, 2006, **8**, 955–966.
- 66 K. Tono, J.-L. Kuo, M. Tada, K. Fukazawa, N. Fukushima, C. Kasai and K. Tsukiyama, *J. Chem. Phys.*, 2008, **129**, 084304.
- 67 E. S. Stoyanov, I. V. Stoyanova and C. A. Reed, *Chem. – Eur. J.*, 2008, **14**, 3596–3604.
- 68 M. Meot-Ner, *Chem. Rev.*, 2012, **112**, PR22–PR103.
- 69 J. J. Fifen, M. Nsangou, Z. Dhaouadi, O. Motapon and N.-E. Jaidane, *J. Chem. Theory Comput.*, 2013, **9**, 1173–1181.
- 70 J. J. Fifen, M. Nsangou, Z. Dhaouadi, O. Motapon and N.-E. Jaidane, *J. Chem. Phys.*, 2013, **138**, 184301.
- 71 J. Brudermann, U. Buck and V. Buch, *J. Phys. Chem. A*, 2002, **106**, 453–457.
- 72 U. Buck, C. C. Pradynski, T. Zeuch, J. M. Dieterich and B. Hartke, *Phys. Chem. Chem. Phys.*, 2014, **16**, 6859–6871.
- 73 C. Steinbach, M. Fárník, I. Ettischer, J. Siebers and U. Buck, *Phys. Chem. Chem. Phys.*, 2006, **8**, 2752–2758.
- 74 J. Zischang and M. A. Suhm, *J. Chem. Phys.*, 2014, **140**, 064312–1–5.
- 75 T. Shimamori and A. Fujii, *J. Phys. Chem. A*, 2015, **119**, 1315–1322.
- 76 M. Okumura, L. I. Yeh, J. D. Myers and Y. T. Lee, *J. Chem. Phys.*, 1986, **85**, 2328–2329.
- 77 N. L. Pivonka, C. Kaposta, M. Brümmer, G. von Helden, G. Meijer, L. Wöste, D. M. Neumark and K. R. Asmis, *J. Chem. Phys.*, 2003, **118**, 5275–5278.
- 78 A. M. Ricks, Z. E. Reed and M. A. Duncan, *J. Mol. Spectrosc.*, 2011, **266**, 63–74.
- 79 K. Mizuse and A. Fujii, *Phys. Chem. Chem. Phys.*, 2011, **13**, 7129–7135.
- 80 O. Rodriguez Jr and J. M. Lisý, *J. Phys. Chem. Lett.*, 2011, **2**, 1444–1448.
- 81 P. J. Kelleher, C. J. Johnson, J. A. Fournier, M. A. Johnson and A. B. McCoy, *J. Phys. Chem. A*, 2015, **119**, 4170–4176.
- 82 D. Gerlich, *Phys. Scr.*, 1995, **T59**, 256–263.
- 83 Y.-S. Wang, C.-H. Tsai, Y. T. Lee, H.-C. Chang, J. C. Jiang, O. Asvany, S. Schlemmer and D. Gerlich, *J. Phys. Chem. A*, 2003, **107**, 4217–4225.
- 84 O. V. Boyarkin, S. R. Mercier, A. Kamariotis and T. R. Rizzo, *J. Am. Chem. Soc.*, 2006, **128**, 2816–2817.
- 85 A. Fujihara, N. Noguchi, Y. Yamada, H. Ishikawa and K. Fuke, *J. Phys. Chem. A*, 2009, **113**, 8169–8175.
- 86 J. T. O'Brien and E. R. Williams, *J. Am. Chem. Soc.*, 2012, **134**, 10228–10236.
- 87 J. G. Redwine, Z. A. Davis, N. L. Burke, R. A. Oglesbee, S. A. McLuckey and T. S. Zwier, *Int. J. Mass Spectrom.*, 2013, **348**, 9–14.
- 88 A. B. Wolk, C. Leavitt, E. Garand and M. A. Johnson, *Acc. Chem. Res.*, 2014, **47**, 202–210.
- 89 H. Kang, G. Féraud, C. Dedonder-Lardeux and C. Jouvet, *J. Phys. Chem. Lett.*, 2014, **5**, 2760–2764.
- 90 N. Heine and K. R. Asmis, *Int. Rev. Phys. Chem.*, 2015, **34**, 1–34.
- 91 S. Xu, S. Gozem, A. I. Krylov, C. R. Christopher and J. M. Weber, *Phys. Chem. Chem. Phys.*, 2015, **17**, 31938–31946.
- 92 S. Dillinger, J. Mohrbach, J. Hewer, M. Gaffga and G. Niedner-Schatteburg, *Phys. Chem. Chem. Phys.*, 2015, **17**, 10358–10362.
- 93 B. M. Marsh, J. M. Voss and E. A. Garand, *J. Chem. Phys.*, 2015, **143**, 204201.
- 94 Y. Inokuchi, M. Nakatsuma, M. Kita and T. Ebata, *J. Phys. Chem. A*, 2016, **120**, 6394–6401.
- 95 H. Ishikawa, I. Kurusu, R. Yagi, R. Kato and Y. Kasahara, *J. Phys. Chem. Lett.*, 2017, **8**, 2541–2546.
- 96 A. Günther, P. Nieto, D. Müller, A. Sheldrick and O. Dopfer, *J. Mol. Spectrosc.*, 2017, **332**, 8–15.
- 97 C. J. T. de Grotthuss, *Ann. Chim.*, 1806, **58**, 54–73.
- 98 I. Yeh, M. Okumura, J. D. Myers, J. M. Price and Y. T. Lee, *J. Chem. Phys.*, 1989, **91**, 7319–7330.
- 99 D. Marx, M. E. Tuckerman, J. Hutter and M. Parrinello, *Nature*, 1999, **397**, 601–604.
- 100 J.-C. Jiang, Y.-S. Wang, H.-C. Chang, S. H. Lin, Y. T. Lee, G. Niedner-Schatteburg and H.-C. Chang, *J. Am. Chem. Soc.*, 2000, **122**, 1398–1410.
- 101 J. M. Headrick, E. G. Diken, R. S. Walters, N. I. Hammer, R. A. Christie, J. Cui, E. M. Myshakin, M. A. Duncan, M. A. Johnson and K. D. Jordan, *Science*, 2005, **308**, 1765–1769.
- 102 J. R. Roscioli, J. R. McCunn and M. A. Johnson, *Science*, 2007, **316**, 249–254.
- 103 G. E. Doublerly, R. S. Walters, J. Cui, K. D. Jordan and M. A. Duncan, *J. Phys. Chem. A*, 2010, **114**, 4570–4579.
- 104 K. Mizuse and A. Fujii, *J. Phys. Chem. A*, 2012, **116**, 4868–4877.
- 105 N. Heine, M. R. Fagiani, M. Rossi, T. Wende, G. Berden, V. Blum and K. R. Asmis, *J. Am. Chem. Soc.*, 2013, **135**, 8266–8273.

- 106 J. A. Tan and J.-L. Kuo, *J. Phys. Chem. A*, 2015, **119**, 11320–11328.
- 107 O. M. Cabarcos, C. J. Weinheimer, T. J. Martínez and J. M. Lisy, *J. Chem. Phys.*, 1999, **110**, 9516–9526.
- 108 C. A. Corbett, T. J. Martínez and J. M. Lisy, *J. Phys. Chem. A*, 2002, **106**, 10015–10021.
- 109 J. P. Beck and J. M. Lisy, *J. Phys. Chem. A*, 2010, **114**, 10011–10015.
- 110 W. H. Robertson, K. Karapetian, P. Ayotte, K. G. Jordan and M. A. Johnson, *J. Chem. Phys.*, 2002, **116**, 4853–4857.
- 111 R. Ayala, J. M. Martínez, R. R. Pappalardo and E. Sánchez Marcos, *J. Phys. Chem. A*, 2000, **104**, 2799–2807.
- 112 C. Faralli, M. Pagliai, G. Cardini and V. Schettino, *J. Phys. Chem. B*, 2006, **110**, 14923–14928.
- 113 J. A. Draves, Z. Luthey-Schulten, W.-L. Liu and J. M. Lisy, *J. Chem. Phys.*, 1990, **93**, 4589–4602.
- 114 T. J. Selegue and J. M. Lisy, *J. Am. Chem. Soc.*, 1994, **116**, 4874–4880.
- 115 T. J. Selegue, N. Moe, J. A. Draves and J. M. Lisy, *J. Chem. Phys.*, 1992, **96**, 7268–7278.
- 116 C. J. Weinheimer and J. M. Lisy, *J. Phys. Chem.*, 1996, **100**, 15305–15308.
- 117 C. J. Weinheimer and J. M. Lisy, *Int. J. Mass Spectrom. Ion Processes*, 1996, **159**, 197–208.
- 118 M. R. France, S. H. Pulins and M. A. Duncan, *Chem. Phys.*, 1998, **239**, 447–457.
- 119 H. Machinaga, K. Ohashi, Y. Inokuchi, N. Nishi and H. Sekiya, *Chem. Phys. Lett.*, 2004, **391**, 85–90.
- 120 K. Furukawa, K. Ohashi, T. Imamura, J. Sasaki, K. Judai, N. Nishi and H. Sekiya, *Chem. Phys. Lett.*, 2010, **495**, 8–13.
- 121 M. Masamura, *J. Phys. Chem. A*, 2002, **106**, 8925–8932.
- 122 J.-L. Kuo and M. L. Klein, *J. Chem. Phys.*, 2005, **122**, 024516.
- 123 Y. Luo, S. Maeda and K. Ohno, *J. Phys. Chem. A*, 2007, **111**, 10732–10737.
- 124 D. J. Miller and J. M. Lisy, *J. Am. Chem. Soc.*, 2008, **130**, 15381–15392.
- 125 D. J. Miller and J. M. Lisy, *J. Am. Chem. Soc.*, 2008, **130**, 15393–15404.
- 126 X.-B. Wang, K. Kowalski, L.-S. Wang and S. S. Xantheas, *J. Chem. Phys.*, 2010, **132**, 124306.
- 127 C. J. Tainter and J. L. Slinner, *J. Chem. Phys.*, 2012, **137**, 104304.
- 128 K. Ohashi, J. Sasaki, G. Yamamoto, K. Judai, N. Nishi and H. Sekiya, *J. Chem. Phys.*, 2014, **141**, 21307.
- 129 R. Shishido, Y.-C. Li, C.-W. Tsai, D. Bing, A. Fujii and J.-L. Kuo, *Phys. Chem. Chem. Phys.*, 2015, **17**, 25863–25876.
- 130 C. T. Wolke, F. S. Menges, N. Totsch, O. Gorlova, J. A. Fournier, G. H. Weddle, M. A. Johnson, N. Heine, T. K. Esser, H. Knorke, K. R. Asmis, A. B. McCoy, D. J. Arismendi-Arrieta, R. Prosmiti and F. Paesani, *J. Phys. Chem. A*, 2015, **119**, 1859–1866.
- 131 M. R. Fagiani, H. Knorke, T. K. Esser, N. Heine, C. T. Wolke, S. Gewinner, W. Schöllkopf, M.-P. Gaigeot, R. Spezia, M. A. Johnson and K. R. Asmis, *Phys. Chem. Chem. Phys.*, 2016, **18**, 26743–26754.
- 132 A. Malloum, J. J. Fifen, Z. Dhaouadi, S. G. N. Engo and N.-E. Jaidane, *Phys. Chem. Chem. Phys.*, 2016, **18**, 26827–26843.
- 133 C. P. Brock and L. L. Duncan, *Chem. Mater.*, 1994, **6**, 1307–1312.
- 134 P. A. McGregor, D. R. Allan, S. Parson and S. J. Clark, *Acta Crystallogr., Sect. B: Struct. Sci.*, 2006, **62**, 599–605.
- 135 Ó. Gálvez, B. Maté, B. Martín-Llorente, V. J. Herrero and R. Escrivano, *J. Phys. Chem. A*, 2009, **113**, 3321–3329.
- 136 P. Derollez, A. Hédoux, Y. Guinet, F. Danède and L. Paccou, *Acta Crystallogr., Sect. B: Struct. Sci., Cryst. Eng. Mater.*, 2013, **69**, 195–202.
- 137 R. Laenen, K. Simeonidis and R. Ludwig, *J. Chem. Phys.*, 1999, **111**, 5897–5904.
- 138 M. Huelsekopf and R. Ludwig, *J. Mol. Liq.*, 2002, **98–99**, 163–171.
- 139 I. León, J. Millán, E. J. Cocinero, A. Lesarri and J. A. Ferández, *Angew. Chem., Int. Ed.*, 2013, **52**, 7772–7775.
- 140 I. León, R. Montero, A. Longarte and J. A. Ferández, *Phys. Chem. Chem. Phys.*, 2015, **17**, 2241–2245.
- 141 Q.-C. Nguyen, Y.-S. Ong and J.-L. Kuo, *J. Chem. Theory Comput.*, 2009, **5**, 2629–2639.
- 142 Q.-C. Nguyen, Y.-S. Ong, H. Soh and J.-L. Kuo, *J. Phys. Chem. A*, 2008, **112**, 6257–6261.
- 143 H. Soh, Y.-S. Ong, Q.-C. Nguyen, Q. Huy, N. M. Salahuddin, T. Hung and J.-L. Kuo, *IEEE Trans. Evol. Comput.*, 2010, **14**, 419–437.
- 144 D. Bing, T. Hamashima, C.-W. Tsai, A. Fujii and J.-L. Kuo, *Chem. Phys.*, 2013, **421**, 1–9.
- 145 D. J. Wales and I. Ohmine, *J. Chem. Phys.*, 1993, **98**, 7245–7256.
- 146 F. Calvo, J. P. K. Doye and D. J. Wales, *Chem. Phys. Lett.*, 2002, **366**, 176–183.
- 147 T. V. Bogdan, D. J. Wales and F. Calvo, *J. Chem. Phys.*, 2006, **124**, 044102–1–13.
- 148 M. Miyazaki, A. Fujii and N. Mikami, *J. Phys. Chem. A*, 2004, **108**, 8269–8722.
- 149 N. R. Samala and N. Agmon, *J. Chem. Phys.*, 2017, **147**, 234307.
- 150 R. Ludwig, *ChemPhysChem*, 2005, **6**, 1376–1380.
- 151 R. Ludwig, F. Weinhold and T. C. Farrar, *Mol. Phys.*, 1999, **97**, 465–477.
- 152 R. Ludwig, F. Weinhold and T. C. Farrar, *Mol. Phys.*, 1999, **97**, 479–486.
- 153 D. Bing, J.-L. Kuo, K. Suhara, A. Fujii and N. Mikami, *J. Phys. Chem. A*, 2009, **113**, 2323–2332.
- 154 M. Katada, P.-J. Hsu, A. Fujii and J.-L. Kuo, *J. Phys. Chem. A*, 2017, **121**, 5399–5413.
- 155 C. C. Pradyznski, R. M. Forck, T. Zeuch, P. Slavíček and U. Buck, *Science*, 2012, **337**, 1529–1532.
- 156 M. Katada, R. Shishido and A. Fujii, *Phys. Chem. Chem. Phys.*, 2014, **16**, 7595–7601.
- 157 R. A. Mata and M. A. Suhm, *Angew. Chem., Int. Ed.*, 2017, **56**, 11011–11018.
- 158 S. Oswald and M. A. Suhm, *Angew. Chem., Int. Ed.*, 2017, **56**, 12672–12676.

- 159 A. Poblotzki, H. C. Gottschalk and M. A. Suhm, *J. Phys. Chem. Lett.*, 2017, **8**, 5656–5665.
- 160 R. A. Provencal, R. N. Casaes, K. Roth, J. B. Paul, C. N. Chapo, R. J. Saykally, G. S. Tschumper and H. F. Schaefer III, *J. Phys. Chem. A*, 2000, **104**, 1423–1429.
- 161 P.-G. Jönsson, *Acta Crystallogr., Sect. B: Struct. Crystallogr. Cryst. Chem.*, 1976, **32**, 232–235.
- 162 M. Ramírez-Cardona, L. Ventolá, T. Calvet, M. A. Cuevas-Diarte, J. Rius, J. M. Amigó and M. M. Reventós, *Powder Diffr.*, 2005, **20**, 311–315.
- 163 S. Naya, *Prog. Theor. Phys.*, 1972, **48**, 407–432.
- 164 V. S. Jorish and V. Y. Zitserman, *Chem. Phys. Lett.*, 1975, **34**, 378–381.
- 165 M. Schwarz Jr, *J. Stat. Phys.*, 1976, **15**, 255–261.